7/24/2002- 1:00 PM
LBNL Report No. LBNL-51149

FATIGUE OF BRITTLE MATERIALS

Robert O. Ritchie

Materials Sciences Division, Lawrence Berkeley National Laboratory, and
Department of Materials Science and Engineering
University of California, Berkeley, CA 94720-1760

Comprehensive Structural Integrity
Edited by I. Milne, R. O. Ritchie, and B. L. Karihaloo
Volume 4 (Cyclic Loading and Fatigue)
Edited by R. O. Ritchie and Y. Murakami

July 2002

Work supported by the Office of Science, Office of Basic Energy Sciences, Division of Materials Sciences and Engineering of the U.S. Department of Energy under Contract No. DE-AC03-76SF00098.

4.12

Fatigue of Brittle Materials

R. O. RITCHIE

Materials Sciences Division, Lawrence Berkeley National Laboratory, and Department of Materials Science and Engineering, University of California, Berkeley, CA 94720-1760, U.S.A.

Contents

4.12.1. INTRODUCTION

The quest for structural materials that can operate at higher and higher temperatures remains a persistent challenge in materials science. To achieve major increases in service temperatures, e.g., for aerospace propulsion systems, ceramic- and intermetallic-matrix composites offer perhaps the best prospects, although their cost is often prohibitive for many applications. For this reason, much recent work has focused on their monolithic counterparts. Despite significant advances in the development of such monolithic ceramics and intermetallics for structural use, their widespread adoption has been severely limited by their generally low ductility and poor fracture toughness, particularly at lower temperatures. In addition, it is now appreciated that these materials can be susceptible to premature failure by cyclic fatigue.

Fatigue involves the microstructural damage and failure of materials under cyclically varying loads. Structural materials, however, are rarely designed with compositions and microstructures optimized for fatigue resistance. Metallic alloys are generally designed for strength, intermetallics for ductility, and ceramics for toughness; yet, if any of these materials see engineering service, their structural integrity is often limited by their mechanical performance under cyclic loads. In fact, it is generally considered that over 80% of all service failures can be traced to mechanical fatigue, whether in association with cyclic plasticity, sliding or physical contact (fretting and rolling contact fatigue), environmental damage (corrosion fatigue), or elevated temperatures (creep fatigue). Consequently, a large volume of literature has been amassed particularly over the past twenty-five years, dealing with the mechanics and mechanisms of mechanical fatigue failure [e.g., 1,2], although the vast majority of this research pertains solely to metallic materials.

Despite this wealth of information on metal fatigue, there has been an increasing interest in the use of high-strength, brittle materials, such as ceramics, intermetallics and their respective composites, for structural applications where cyclic loading is critical [e.g.,3,4]. This has been particularly centered on high temperature applications, e.g., for fuselage and especially engine components [4], but in the case of ceramics at lower temperatures too, e.g., for biomedical implant devices [5]. Examples of such "advanced materials" are the use of silicon nitride ceramics for automobile turbocharger wheels and engine valves and pyrolytic carbon for prosthetic cardiac devices, and the contemplated use of composite ceramics in gas turbine engines. Similarly, intermetallic alloys, such as the γ-based titanium aluminides, have been considered for applications such as valves in automobile engines and low-pressure blades in gas turbines. Whereas these materials offer vastly improved specific strength at high temperatures compared to conventional metallic alloys, they suffer in general from a pronounced lack of damage tolerance in the form of an extreme sensitivity to pre-existing flaws. Moreover, as noted above, it has become apparent that similar to metals, such brittle solids can additionally show a marked susceptibility to premature failure under cyclic fatigue loading [e.g.,6].

The mechanisms involved in the propagation of fatigue cracks in brittle materials are quite distinct from those commonly encountered in metal fatigue; moreover, their crack-growth rate (*da/dN*) behavior displays a markedly higher sensitivity to the applied stress intensity (*K*) than is observed in most metals (Fig. 1) [7-9]. However, by considering crack growth as a mutual competition between *intrinsic* microstructural damage mechanisms, which promote crack extension *ahead* of the tip, and *extrinsic* crack-tip shielding mechanisms, which act primarily *behind* the tip to retard crack growth [8], a specific commonality of behavior between the fatigue of ductile and brittle materials can be found, differing only in the relative importance of the intrinsic and extrinsic mechanisms.

4.12.2. INTRINSIC AND EXTRINSIC MECHANISMS

The extension of a crack can be considered to be a result of the mutual competition of two classes of mechanisms (Fig. 2). Crack growth is promoted *ahead* of the crack tip by *intrinsic* microstructural damage mechanisms, and impeded by *extrinsic* mechanisms acting primarily *behind* the crack tip, which serve to "shield" the crack tip from the far-field driving force [8].

Intrinsic damage mechanisms in metallic materials typically involve processes which create microcracks or voids, e.g., by dislocation pile-ups or interface decohesion, in the highly stressed region ahead of the tip, leading to classical failure by cleavage, intergranular cracking or microvoid coalescence; comparable mechanisms under cyclic loads involve the repetitive blunting and resharpening of the crack tip [e.g.,10,11]. Extrinsic shielding mechanisms, conversely, result from the creation of inelastic zones surrounding the crack wake or from physical contact between the crack surfaces via wedging, bridging, sliding or combinations thereof (Fig. 3) [8]. Examples of "zone shielding" are transformation and microcrack toughening in ceramics and rocks, where the *in situ* dilatant phase transformations or the microcracking of precipitates/particles ahead of the crack tip can lead to inelastic zones in the crack wake which impart closing tractions on the crack surfaces. Examples of "contact shielding" are the bridging tractions imposed across a crack by unbroken fibers, laminated layers or a particulate phase in composite materials, or the wedging of corrosion debris or fracture surface asperities during crack closure in metal fatigue.

Intrinsic mechanisms are an inherent property of the material, and thus are active irrespective of the length of the crack or the geometry of the test specimen; under monotonic loads, for example, they control the driving forces (e.g., the stress intensity) to *initiate* cracking. Extrinsic mechanisms, conversely, act in the crack wake and are thus critically dependent on crack size and (to a lesser extent) geometry; they are responsible for the development of resistance-curve (R-curve) behavior and thus play a prominent role in the driving forces required for continued *growth* of the crack. The implications of this are that where extrinsic shielding mechanisms are active, rising R-curve toughness behavior and "small-crack" effects are to be expected, both phenomena resulting from the crack-growth properties being dependent upon crack size. Moreover, since extrinsic

mechanisms can have no effect on crack initiation (since there is no crack wake), the microstructural factors affecting (large) crack growth may be quite different from those affecting crack initiation (or small crack growth).

In general, ductile materials are toughened intrinsically, e.g., through mobile dislocation activity to induce a significant plastic-zone size, although under cyclic loading extrinsic mechanisms play an important role in the form of crack closure. In contrast, brittle materials, such as ceramics, are invariably toughened extrinsically [e.g., 12,13], via such mechanisms as transformation toughening and crack bridging, the latter through interlocking grains in many monolithic ceramics or by uncracked ligaments or unbroken reinforcement phases in composites and laminates.

In terms of finding any commonality in mechanisms of fatigue-crack growth in different materials, *it is the specific nature and, more significantly, the relative importance of the intrinsic (damage) versus extrinsic (shielding) mechanisms which distinguishes the cyclic fatigue behavior of ductile and brittle solids.* This in turn governs the specific dependencies of the alternating and maximum stress intensities on crack-growth rates, i.e., how da/dN depends upon ΔK and K_{max} (and thus how the resulting lifetime is a function of the alternating or maximum stresses), and the relationships between the thresholds for fatigue-crack growth (ΔK_{TH} and $K_{max,TH}$) and the crack-initiation (K_o) and steady-state (K_c) fracture toughness values [9].

However, prior to describing the mechanics and mechanisms affecting cyclic crack growth in brittle materials, we begin with a brief review of ductile materials.

4.12.3. FATIGUE-CRACK GROWTH IN METALLIC MATERIALS

4.12.3.1. General Considerations

Fatigue-crack growth can occur at stress intensity K levels generally far less than the fracture toughness, K_c, in any metallic alloy when cyclic loading is applied ($\Delta K_{TH}/K_c \sim$ 0.1 - 0.4). Stated simply, the accumulation of damage from the cyclic plastic deformation in the plastic zone at the crack tip accounts for the intrinsic mechanism of fatigue crack growth at K levels below K_c. The process of fatigue failure itself consists of several processes involving initial cyclic damage (cyclic hardening or softening), formation of an initial "fatal" flaw (crack initiation), macroscopic propagation of this flaw (crack growth), and final catastrophic failure or instability.

The problem of fatigue failure was first seriously considered in the mid nineteenth century when widespread failures of railcar axles in Europe prompted Wöhler in Germany to conduct the first systematic investigations into material failure under cyclic stresses *circa* 1860 [14]. However, the main impetus for research directed at the crack propagation stage of fatigue failure, as opposed to mere lifetime calculations, did not occur until the mid 1960s, when the concepts of linear elastic fracture mechanics and so-called "defect-tolerant design" were first applied to the problem of subcritical flaw growth [15,16]. Such approaches recognize that all structures are flawed, and that cracks

may initiate early in service life and propagate subcritically. Lifetime is then assessed on the basis of the time or number of loading cycles for the largest undetected crack to grow to failure, as might be defined by an allowable strain, or limit load, or K_c criterion. Implicit in such analyses is that subcritical crack growth can be characterized in terms of some governing parameter (often thought of as a crack driving force) that describes local conditions at the crack tip yet may be determined in terms of loading parameters, crack size, and geometry. Linear elastic and nonlinear elastic fracture mechanics have, to date, provided the most appropriate methodology for such analyses to be made.

The general aspects of fatigue-crack growth in metallic materials and its description using fracture mechanics can be briefly summarized by the schematic diagram in Fig. 4 showing the variation in da/dN with the nominal stress-intensity range ($\Delta K = K_{max} - K_{min}$) [17]. In actuality, the growth rates depend upon numerous factors other than ΔK, although this is the primary variable in metal fatigue, viz.:

$$da/dN = f\,[\Delta K, K_{max}\ (\text{or } R), \nu, \text{environment, wave form } \ldots.] \,, \qquad (1)$$

where the load ratio R is the ratio of minimum to maximum applied loads ($= K_{min}/K_{max}$ for positive R), and ν is the frequency. Specifically, results of fatigue-crack growth rate tests for most ductile materials display the following characteristics: (i) a region at low values of ΔK and da/dN (less than $\sim 10^{-9}$ m/cycle) in which fatigue cracks appear dormant below the fatigue thresholds, ΔK_{TH} and $K_{max,TH}$; (ii) an intermediate region ($\sim 10^{-9}$ to 10^{-6} m/cycle) of power-law behavior nominally described by the Paris equation [16]:

$$da/dN = C(\Delta K)^m \,, \qquad (2)$$

where C and m ($\sim$ 2 to 4) are material scaling constants; and (iii) an upper region of accelerating crack growth (above $\sim 10^{-6}$ m/cycle) as K_{max} approaches K_c or gross plastic deformation of the specimen (the limit load). Similar approaches have been suggested for crack growth under large-scale yielding [e.g., 18] where growth rates have been related to a cyclic J-integral (ΔJ) or range of crack-tip opening displacement (ΔCTOD).

4.12.3.2. Mechanistic Aspects

4.12.3.2.1 Intrinsic mechanisms

Ideally, fatigue failure in metals can be characterized by a transgranular ductile striation mechanism, although in many materials they are difficult to identify due to nature of the underlying microstructure or the occurrence of other cracking modes. Striations represent *local* crack-growth increments per cycle and have been hypothesized to occur via a mechanism of opening and blunting of the crack tip on loading, followed by resharpening of the tip on unloading [19]. Several theoretical models for such growth (often termed stage II crack propagation) have been proposed that rely on the fact that, where plastic zones are sufficiently large compared to microstructural dimensions, plastic blunting at the crack tip is accommodated by shear on two slip-systems roughly 45° to

the crack plane [10,11]. Recognizing that such sliding-off is largely irreversible, new crack surface can be created during cyclic crack advance either by simultaneous or alternating slip on these two systems. This damage process is the primary intrinsic mechanism promoting crack advance.

Simple models for striation formation [e.g., 20] predict that an upper-bound estimate for the increment of crack advance per cycle should be proportional to the cyclic crack tip opening displacement (ΔCTOD):

$$\frac{da}{dN} \propto \Delta\text{CTOD} \approx \beta \frac{\Delta K^2}{2\sigma_0 E'} \quad , \tag{3}$$

where σ_o and E' are respectively the appropriate flow stress and Young's modulus, and β is a proportionality constant, of order 0.1-0.5, reflecting the efficiency of crack-tip blunting and reversibility of slip. This approach provides a first-order description of crack-growth rate behavior in the mid-range of growth rates (regime B in Fig. 4), as shown for example by recent results on a bulk amorphous Zr-TiCu-Ni-Be metal where crack advance occurs by a striation mechanism (Fig. 5) [21], although it is an insufficient description at high growth rates and in the near-threshold regime.

At high growth rates as $K_{max} \rightarrow K_c$ (regime C in Fig. 4), the simple Paris law (Eq. 2) underestimates measured growth rates due to the occurrence of monotonic fracture mechanisms (static modes) which replace, or are additional to, striation growth. Such mechanisms include cleavage, intergranular cracking and microvoid coalescence and their presence results in growth rates that are markedly sensitive to microstructure and K_{max} (or R) [22]. Conversely, at very low growth rates where $\Delta K \rightarrow \Delta K_{TH}$ (regime A in Fig. 4), the Paris law overestimates measured growth rates and behavior becomes markedly sensitive to K_{max}, microstructure and environment; the K_{max} dependence in this regime, however, results primarily from crack closure. At such near-threshold levels, the scale of local plasticity (i.e., the plastic-zone size, r_y) approaches microstructural size-scales, and measured growth rates become less than an interatomic spacing per cycle, indicating that crack advance is not occurring uniformly over the entire crack front [e.g., 17]. Crack-growth mechanisms in this regime (typically where r_y is smaller than the grain size) generally are faceted [e.g.,23], often being referred to as "microstructurally sensitive" or "crystallographic" fatigue, and reflect more of a single shear mode of crack advance with associated mode II plus mode I displacements, particularly in coarse planar-slip materials.

4.12.3.2.2 Extrinsic mechanisms

Although the primary mechanism motivating fatigue-crack extension in ductile materials, i.e., crack-tip blunting and resharpening, is intrinsic and controlled principally by ΔK (or more precisely the local plastic strain range), extrinsic crack closure mechanisms act in the crack wake to oppose this. Such wedge shielding [8] results from local deformation, fracture and chemical processes which induce physical contact between the mating crack

surfaces at positive loads during the fatigue cycle. Elber [24] originally proposed that closure arises from the constraint of surrounding elastic material on the residual stretch in material elements previously plastically strained at the tip (*plasticity-induced closure*). Since the crack cannot propagate while it remains closed, the net effect is to reduce the nominal (applied) ΔK value to some lower effective (local) value ΔK_{eff} actually experienced at the crack tip:

$$\begin{aligned} \Delta K_{\text{eff}} &= K_{\max} - K_{\text{cl}}, \qquad (K_{\min} \le K_{\text{cl}}) \\ &= K_{\max} - K_{\min}, \qquad (K_{\text{cl}} \le K_{\min}) \end{aligned} \tag{4}$$

where K_{cl} is the stress intensity to close the crack. There are, however, several mechanisms of closure which assume greater importance at near-threshold levels, where CTODs are small and approach the dimensions of the "wedge". These processes rely on wedging mechanisms inside the crack from corrosion debris, fracture surface asperities, or, in the case of environmentally assisted fatigue, fluid inside the crack, as reviewed in ref. [25].

Crack closure arising from crack-surface corrosion deposits (*oxide-induced closure*) is promoted in oxidizing environments at low load ratios. Notable examples are the crack surface oxides and calcareous deposits formed during corrosion fatigue in structural steels tested, respectively, in water and sea water, and the chromic oxides formed during creep fatigue in Ni-based superalloys. Simple quantitative modeling, based on the concept of a rigid wedge inside a linear elastic crack, suggests that such closure depends upon the thickness d of the oxide film and the location of its peak thickness from the crack tip $2z$ [25]:

$$K_{\text{cl}} \approx \frac{E'd}{4\sqrt{\pi z}}, \tag{5}$$

implying that deposits in the immediate vicinity of the crack tip will have a dominating influence in the development of closure by this mechanism. A more general source arises from the wedging action of fracture surface asperities, where CTODs are small and where significant crack-tip shear displacements occur. Such *roughness-induced closure* is promoted at near-threshold levels, particularly where crack advance is strongly crystallographic, as in coherent-particle-hardened (planar slip) systems such as underaged Al alloys and Ni-based superalloys or in duplex microstructures where the crack can be made to meander from frequent crack deflection. Notable examples of where crack deflection and the resulting closure has led to excellent crack growth properties are found with dual-phase steels, β-annealed Ti alloys and Al-Li alloys. The magnitude of roughness-induced mechanism depends upon the degree of fracture surface roughness and the extent of the mode II crack-tip displacements. From simple two-dimensional geometric modeling, the closure stress intensity at the point of first asperity contact is given as [25]:

$$K_{cl} \approx \sqrt{\frac{2\gamma u}{1+2\gamma u}} K_{max} \quad , \tag{6}$$

where γ is a measure of surface roughness, that is, ratio of height to width of the asperities, and u is the ratio of mode II to mode I displacements.

Because crack closure mechanisms involve a wedging process which effectively raises the minimum stress intensity, the potency of the shielding depends upon the magnitude of the crack-tip opening displacement compared to the dimension of the wedge. Since CTODs are much larger at R, the closure effect is markedly diminished at high load ratios, i.e., it is controlled primarily by the value of K_{max}, particularly at lower ΔK levels, where closure results predominantly from oxide or asperity wedging. Thus, in the fatigue of ductile materials, it is the ΔK-component of the driving force which controls the intrinsic damage mechanisms ahead of the crack tip[1], whereas the K_{max}-component controls the extrinsic shielding mechanisms behind the tip.

4.12.4. FATIGUE-CRACK GROWTH IN CERAMIC MATERIALS

4.12.4.1 General Considerations

Extrinsic mechanisms are far more important in the toughening of materials with little or no ductility. Indeed, intrinsic toughening mechanisms, to promote crack-tip plasticity, for example, have been largely unsuccessful in brittle solids such as glasses and ceramics. Instead, ceramic materials have been toughened using a variety of crack-tip shielding mechanisms (Fig. 6) [e.g.,12,13]. Their effect is to impede crack extension via mechanical, microstructural and environmental factors that *locally* reduce the near-tip stress intensity, i.e., to promote R-curve toughening.

For example, although the intrinsic toughness of zirconia is only ~2 MPa√m, by inducing an *in situ* phase transformation at the crack tip (transformation toughening) or by causing the *in situ* microcracking of particles (microcrack toughening), both processes causing a dilation around the crack tip which is constrained by surrounding elastic material, the measured K_c can be raised extrinsically to between 8 and 15 MPa√m [e.g.,12]. Similarly, by inducing crack branching and meandering, due to crack deflection at particles or interfaces, three-fold increases in toughness can be obtained. Composites can be also toughened by crack-tip shielding mechanisms; a potent form is through crack bridging where cracks are bridged by intact brittle fibers or whiskers, or are made to intersect a ductile phase that undergoes plastic deformation as the crack passes [e.g.,12,13].

By designing microstructures that develop such shielding processes, monolithic and composite ceramics can now be processed with toughnesses up to an order of magnitude higher than was available 20 or so years ago. It is perhaps ironic, however, that whereas

[1] The exception to this is behavior at high stress intensities as K_{max} approaches K_c or the limit-load instability (Regime C in Fig. 4), where additional static fracture mechanisms (e.g., cleavage, microvoid coalescence) occur; these mechanisms are primarily K_{max} controlled [22].

glasses and untoughened ceramics are essentially immune to cyclic fatigue [26],[2] the generation of a nonlinear stress-strain curve with toughened ceramics results in their susceptibility to premature fatigue failure under cyclic loading.

The characteristics of cyclic fatigue in ceramics appear to be quite different to that of metal fatigue:

1. Unlike in ductile materials and with the exception of phase-transforming ceramics such as PSZ [29], fatigue cracks in ceramics do not appear to initiate naturally; crack initiation is invariably associated with some pre-existing defect.
2. Again unlike metal fatigue where there is a characteristic fracture mode for cyclic loading, i.e., striation growth, which is quite distinct from that for monotonic loading, the morphology of fatigue fracture surfaces in ceramics is almost identical to that under monotonic loads, although more debris is often present on the fatigue fractures. Indeed, the crack path and crack-advance mechanism appear to be identical under static and cyclic loading [30] (Fig. 7).
3. Microstructure can have a significant effect on fatigue-crack growth rates in ceramics [7,30], as for example shown by the variation in da/dN with ΔK for a series of partially-stabilized zirconias (Mg-PSZ) with increasing R-curve toughness, resulting from a larger extent of transformation toughening [7]. However, by plotting these results in terms of the effective near-tip stress intensity, which in this case is equivalent to normalizing the data in terms of the fracture toughness, i.e., by characterizing the growth rates with K_{max}/K_c, the microstructural effects are essentially removed (Fig. 8). This implies that unlike metals, the microstructural influences on fracture by fatigue are similar to those for overload fracture.
4. The sensitivity of growth rates to the stress intensity is extremely high; specifically, the exponent m in the simple Paris equation (Eq. 2) can take values as high as ~15 to 50 and above [7], as shown by the growth-rate curves for alumina, PSZ and pyrolytic carbon in Fig. 1. The very high exponents, however, result from a particularly marked sensitivity of growth rates to K_{max}, rather than ΔK *per se*. This can be appreciated by expressing the growth-rate relationship in terms of both K_{max} and ΔK, viz [31,32]:

$$da / dN = C'(K_{max})^n (\Delta K)^p \quad , \tag{7}$$

where, compared to Eq. 2, C' is a constant equal to $C(1 - R)^n$ and $(n + p) = m$. In a typical brittle ceramic, e.g., SiC-whisker reinforced Al_2O_3, the exponents n and p are ~10 and 5 [31], respectively; this is to be compared with values of $n = 0.5$ and $p = 3$ for metal fatigue of a nickel-base superalloy [32].

4.12.4.2 Mechanistic Aspects

[2] Whereas mechanical fatigue is generally non-existent in amorphous glasses and untoughened ceramics, recent studies have identified fatigue effects in borosilicate glass at near-threshold growth rates [27] and premature fatigue failures in micron-scale silicon thin films [28], both phenomena which have been attributed to environmental processes such as the entrapment of reacting water molecules and the environmentally-assisted cracking of the native oxide layer.

Mechanistically, it is clear that fatigue-crack advance in ceramics is conceptually different from that in metals. Again we can involve the intrinsic vs. extrinsic concept to explain this distinction. Essentially, there are two possible classes of fatigue mechanisms (where failure is associated with a dominant crack): (i) *intrinsic mechanisms* where, as in metals, crack advance results from damage processes in the crack-tip region, which are unique to cyclic loading, and (ii) *extrinsic mechanisms*, where the crack-advance mechanism ahead of the crack tip is identical to that for monotonic loading, but the unloading cycle promotes accelerated crack growth by degrading the degree of crack-tip shielding behind the tip.

Whereas the cyclic processes in metal fatigue are predominantly intrinsic in nature, the cyclic fatigue processes in ceramics are extrinsic. The mechanism by which the crack advances is thus identical under cyclic loading as it would be in a single overload cycle; this clearly is consistent with the marked dependency of growth rates on K_{max} (rather than on ΔK) and a similarity in fracture surface appearance under cyclic and monotonic loading. The cyclic loading conversely acts to diminish the shielding (i.e., the R-curve toughening) in the crack wake. This can take various forms depending upon the prevailing shielding mechanism; examples include the premature fatigue failure of metallic reinforcement phase in ductile-phase toughened materials [34,35], a reduction in the effect of fiber bridging in fiber-reinforced ceramic-matrix composites [36], and a decreased bridging capacity of a wake zone of interlocking grains in grain-bridging ceramics, such as coarse-grained Al_2O_3, grain-elongated Si_3N_4, and *in situ* toughened SiC [37-41].

As an example of this phenomenon, the latter mechanism of a fatigue-induced reduction in grain bridging in monolithic ceramics is considered (Fig. 9). As the decay in bridging is associated with the relative motion of the grains as the crack proceeds intergranularly, this can be modeled in terms of cycle-dependent sliding wear degradation of frictional grain bridges [38].

Specifically, where thermal expansion anisotropy results after processing in certain grains experiencing residual compression, cracks will extend preferentially in the tensile regions surrounding the grain, leaving it intact and spanning the crack. The resulting closing traction on the crack surfaces, the grain bridging stress, p, can be expressed as a function of the distance behind the crack tip, X, and the crack-opening displacement, $2u$, in terms of the length of the bridging zone, L, and an exponent, k, as [12,42-45]:

$$p(X) = P_{max}\,(1 - X/L)^k \quad ,$$

$$p(u) = P_{max}\,(1 - X(u)/L)^k \quad . \tag{8}$$

The function $p(X)$ describes the bridging stress distribution as a function of distance behind the crack tip, X, starting from a maximum value of P_{max} at the crack tip ($X = 0$), and falling to zero at the end of the bridging zone ($X = L$), where $2u = 2u_f$, the critical crack-opening for bridge rupture. The maximum bridging stress is related to the residual

stresses and is equivalent to the product of the residual clamping stress acting on a grain, σ_N, due to thermal expansion anisotropies and the coefficient of friction, μ, i.e., $P_{max} = \mu\sigma_N$. The shape of the decrease is determined by the exponent *k;* a uniformly distributed stress over the bridging zone would imply $k = 0$ whereas $k = 1$ corresponds to frictional pullout where the cross-sectional geometry of the bridging grains does not change during crack opening [45].

The bridging stress $p(u)$ rises rapidly with u during debonding of the grain, followed by a gradual decrease where frictional pullout of the grain occurs (Fig. 9); both processes contribute to the toughness, although in general most energy is dissipated during frictional pullout. Under cyclic loads, the repetitive opening and closing of the crack results in a decrease in the toughening capacity of the bridging zone by reducing the grain bridging stress, i.e., accumulated damage at the grain/matrix interface ahead of the tip and reduced frictional sliding resistance of partially debonded grain/matrix interfaces from frictional wear causes premature grain debonding and a reduced frictional pullout stress.

A quantitative verification of this extrinsic mechanism for fatigue-crack growth in ceramics can be derived by measuring the crack-opening profiles of cracks grown at high velocity near the K_c instability (to simulate behavior on the R-curve) and at low velocity near the fatigue threshold (to simulate the cyclically-loaded crack) [41]. The net crack-opening profile, $u(X)$, for a linear-elastic crack under an applied far-field stress intensity, K_A, with a bridging traction distribution, $p(X)$, of length L acting across the crack faces can be expressed, in terms of the elastic modulus E' (= E in plane stress or $E/(1-\nu^2)$ in plane strain; ν is Poisson's ratio), as [46]:

$$u(X) = \frac{K_A}{E'}\left(\frac{8X}{\pi}\right)^{1/2} + \frac{2}{\pi E'}\int_0^L p(X')\,\ln\left|\frac{\sqrt{X'}+\sqrt{X}}{\sqrt{X'}-\sqrt{X}}\right| dX', \qquad (9)$$

where X' is the integrated variable where the stress p acts. The first term in Eq. 9 reflects the *traction free* crack under tensile loading in small-scale yielding [47].

In situ measurements on a loading stage in the scanning electron microscopy on a toughened silicon carbide (ABC-SiC) of the opening profile for a crack approximating R-curve behavior (grown at K_A = 6.22 MPa$\sqrt{m}$ (~92% K_c)) are plotted in Fig. 10a as function of distance X behind the crack tip [41]. Also shown are the best-fit profile determined from Eq. 9 (dashed line) and the calculated opening profile for a traction-free crack (solid line). Using fitting procedures on these data, the best-fit $p(X)$ and $u(X)$ functions can be estimated (Fig. 10b) and used to calculate the $p(u)$ function (Eq. 8), from which the R-curve can be predicted [41]. The bridging contribution for a crack that has propagated an amount Δa, $K_B(\Delta a)$, can be estimated from $p(X)$ via [42]:

$$K_B(\Delta a) = \left(\frac{2}{\pi}\right)^{1/2}\int_0^{\Delta a}\frac{p(X)}{\sqrt{X}}dX \qquad (10)$$

By varying Δa from $\Delta a = 0$ to $\Delta a = L$, and knowing long-crack initiation toughness ($K_0 \sim 5.5$ MPa$\sqrt{\text{m}}$ for ABC-SiC [40]), the resistance curve, $K_R(\Delta a)$, can be determined from:

$$K_R(\Delta a) = K_0 + K_B(\Delta a). \tag{11}$$

Using this analysis, the R-curve for ABC-SiC can be predicted, and has been found to be in reasonable agreement to that measured experimentally on compact-tension specimens [41].

The corresponding opening profile (at $K_A = 6.22$ MPa$\sqrt{\text{m}}$) for a crack grown after extensive fatigue cycling at a near-threshold growth rate of $\sim 1 \times 10^{-10}$ m/cycle is compared in Fig. 10a with the profiles for the traction-free (solid line) and R-curve cracks. It is apparent that the near-threshold crack is significantly more open than the R-curve crack, particularly in the near crack-tip region where most of the steady-state toughness is developed (i.e., within ~ 600 μm of the tip); indeed, the profile is essentially identical to that for the traction-free crack. This is consistent with a reduction in the magnitude of bridging tractions for a bridging zone that has experienced $\sim 10^8$ loading cycles. Best-fit $p(X)$ functions from the fatigue and R-curve cracks are compared in Fig. 10b, and show how continued cyclic loading acts to degrade the bridging tractions [41].

By estimating the magnitude of bridging tractions at several applied K levels using this crack profile method, the cyclic crack growth-rate data can be simulated based on the notion that the crack-advance mechanism does not change and that the influence of the cyclic loads is solely to progressively degrade crack bridging, i.e., the *local* crack-tip stress intensity remains at K_O. Using this approach, the predicted variation in da/dN with ΔK for the ABC-SiC has been found to be in reasonably close agreement with experimentally measured data at $R = 0.1$ [41]. Such direct quantitative evidence of a cycle-induced degradation in shielding imply that the essential physics of the cyclic-crack growth process involves the cycle-dependent degradation of the active bridging zone.

4.12.4.3 Elevated Temperature Behavior

There are far fewer studies on fatigue-crack growth in ceramics at elevated temperatures [30,48-56]. This is associated in part with experimental difficulties encountered at temperatures above ~1000°C. More importantly, however, mechanistic interpretation is considerably more complex due to the appearance of creep damage mechanisms (e.g., grain-boundary cavitation) [57], thermally activated crack growth, and additional crack-tip shielding mechanisms such as viscous phase bridging [58-61]. Studies [55] on a near commercial silicon nitride (NT 164) reveal a small acceleration in growth rates at 800°C (where creep damage is negligible). Presumably this is due to a reduction in grain bridging caused by relaxation of the residual stresses (associated with thermal expansion anisotropy). Between 900° and 1200°C, relaxation of the bridging forces continues and so crack-growth rates are seen to increase. The acceleration is further enhanced above

1000°C with the onset of creep cavitation damage in the grain-boundary (mainly glassy) phase. Above 1200°C, the softening of the grain-boundary phase leads to an additional shielding mechanism, viscous-phase bridging, which acts to impede crack growth and to increase the tendency for crack arrest via crack-tip blunting. Moreover, the viscoelastic nature of the bridging response results in a marked dependence of crack-growth rates on loading frequency.

4.12.4.3.1 Viscous-phase bridging

As the principal shielding mechanism at elevated temperatures is such bridging, several models for viscous-phase shielding have been developed in order to predict the anticipated frequency dependence on growth rates [58-61]. Specifically, a microstructurally-based self-consistent numerical model, which is more fully described in ref. [61], examines in detail the mechanics of the extrinsic viscous-film bridging process (Fig. 11), with specific emphasis on its role in influencing elevated-temperature cyclic fatigue-crack propagation. The model incorporates microstructural parameters such as grain size, viscosity and thickness of the grain-boundary film, as well as external variables such as loading frequency, cyclic load amplitude, and load ratio. Unlike previous high-temperature viscous bridging models which have presumed a parabolic crack-opening profile [58,59], a fully self-consistent numerical approach is adopted (no limiting assumptions are made as to the shape of the profile). Moreover, the model is not based on a viscous fluid film filling the crack (viscous-ligament bridging) [60]. Rather, bridging loads are transmitted across the crack walls due to shear resistance of a grain-boundary film deforming between the matrix and the active bridging grain, allowing for the incorporation of more microstructural detail [61]. Furthermore, instead of seeking a global representation of the effect of the bridging tractions (e.g., $K_B(t)$) from a prescribed displacement distribution, the approach is to consider a displacement distribution self-consistent with the corresponding traction distribution.

The displacements due only to an arbitrary, smooth traction distribution in the wake of a crack, $u^b(x)$, are given by:

$$u^b(x) = \int_0^a \int_x^a G(\alpha, x) G(\alpha, x') p(x') d\alpha \, dx' \tag{12}$$

where G is the appropriate Green's function. For the self-consistent solution, where $p(x)$ is a function of $u(x)$, the following relation must be satisfied:

$$u(x) = u^\infty(x) + u^b(x), \tag{13}$$

where $u^b(x)$ is the contribution to the displacement from the bridging tractions, and $u^\infty(x)$ is the traction-free displacement distribution along the flank of the crack. The grain-boundary phase displacements are divided into elastic- and viscous-based components. The relation between these components is determined by using the equality of the elastic and viscous shear stresses in the grain-boundary phase. Although any appropriate

traction-free, geometry specific, form may be used, the traction-free distribution for a semi-infinite body in plane strain is utilized [47]:

$$u^{\infty}(x) = \frac{K_a}{E'}\sqrt{\frac{8x}{\pi}}\,. \tag{14}$$

Because the displacements due to the bridging tractions depend on the total crack flank opening, a local solution along the flank of the crack is necessary in order to provide a self-consistent solution for any non-trivial problem. The methodology used in this model provides this local solution by discretizing the crack flank and forming a pointwise solution. Where the solution between points is needed, a quadratic interpolation of the solution using the adjacent solution points is used. Furthermore, for all solutions the velocity, $\dot{u}(x)$, was approximated linearly in time.

The overall solutions allow for a complete description of the crack-opening displacements, $u(x)$, bridging stress distributions, $p(x)$, crack bridging terms, $K_B(t)$, and crack-tip loading conditions, $K_{tip}(t)$, throughout the loading history. Results from the self-consistent solutions [61] are presented in Fig. 12 by showing changes in the normalized crack-tip loading (K_{max}/K_m, K_{min}/K_m) at steady state versus changes in the model parameters. Crack-tip shielding from bridging is seen to increase with (a) grain-aspect ratio, d/h, (b) viscosity, η, and (c) test frequency, f, for a fixed set of other parameters. Clearly, viscous-film bridging is a potentially effective shielding mechanism that can markedly reduce the stress intensity actually experienced at the crack tip during cyclic fatigue at elevated temperatures (Fig. 12).

A closed-form solution to a simplified version of the bridging model is possible when a parabolic, K_{tip}-controlled displacement distribution is assumed. This solution yields an appropriate non-dimensional group for characterizing the results of the self-consistent calculations given by:

$$\Gamma = \frac{16A_f\eta d l_b f}{\delta h E}\,. \tag{15}$$

where A_f is the area fraction of bridging ligaments, l_b is the bridging-zone length, E is Young's modulus, and δ is the grain-boundary width. A comparison of the trends predicted using self-consistent and parabolic solutions is presented in Fig. 13 by plotting the normalized crack-tip cyclic loading versus the non-dimensional group, Γ, which is a function of the primary model parameters. This allows a judgment to be made as to the appropriateness of Γ as a characterizing parameter. It is evident that the parameter, Γ, normalizes the results over the entire range of the parameters studied here and acts as an appropriate non-dimensional grouping. Indeed, an order of magnitude trade-off exists between the various parameters of the model. For example, an increase in the viscosity by a factor of ten would have exactly the same effect as a decrease in the frequency by a factor of ten.

Similar to the parabolic approximation, for the self-consistent solution the normalized cyclic loading rapidly changes over the range $1 < \Gamma < 100$ from full to very low transmission of the applied loading to the crack tip. At low Γ, the self-consistent and parabolic solutions converge as expected, with the latter solution being quite robust between $0.1 < \Delta K_{tip}/\Delta K_a < 0.9$. At high Γ, where the bridging tractions are largest, the two solutions diverge with the parabolic solution over-predicting the dampening effect of the bridging zone.

Due to the sensitivity of the solutions to Γ, changes in test frequency and temperature (through the viscosity) would appear to be the most likely of the model variables affecting the crack-tip loading conditions in testing or service. Indeed, recent results [62] on elevated-temperature cyclic fatigue-crack propagation in gas-pressure sintered EC-14 silicon nitride display a marked effect of frequency (2-20 Hz) at both 1200° and 1300°C (Fig. 14). While considerations relating to applied loading frequency can be anticipated directly from the solutions presented here, it is not possible to be fully quantitative at this stage since the frequency also has a marked influence on the degree of intrinsic creep damage. Incorporating both intrinsic and extrinsic components into a crack-growth relationship for fatigue cracks in ceramics at elevated temperatures must await further modeling studies.

4.12.4.3.2 Crack-growth behavior

Fatigue-crack propagation in ceramics at high homologous temperatures invariably involves significant contributions from creep mechanisms, such as softening of the amorphous grain-boundary films and cavitation damage there. Indeed, there is often a major compromise in the design of ceramic microstructures, as optimum low-temperature toughness is generally achieved with the grain-boundary glassy films to promote intergranular cracking and hence grain bridging, whereas optimum high-temperature properties are generally achieved in the absence of such films, as they are preferred sites for creep damage. Examples of the former case are many silicon nitride ceramics and ABC-SiC, as discussed above in section 4.12.4.2, whereas commercial SiC (Hexaloy SA) is an excellent example of the latter, having very poor room-temperature toughness but exceptional high-temperature properties.

One ceramic where simultaneous enhancements in low-temperature toughness and high-temperature strength, fatigue and creep resistance have been achieved is ABC-SiC [63]. Essential to the success of simultaneously retaining these properties in this material is the creation of a grain-boundary film that crystallizes at high temperatures and retains a stable structure and composition (Fig. 15). As described below, the crystalline boundary films in ABC-SiC, which form in *situ* or can be produced by prior high-temperature annealing, are less prone to softening and are far more resistant to cavitation; moreover, they do not appear to degrade the subsequent low-temperature strength or toughness [64].

Fig. 16 illustrates the variation in fatigue-crack growth rates with the applied ΔK (at a load ratio of 0.1) for ABC-SiC for temperatures between ambient and 1300°C at a range

of loading frequencies from 3 to 1000 Hz [30,63]. Akin to behavior at lower temperatures, crack-growth rates above 850°C display a marked sensitivity to the stress intensity regardless the loading frequency; in terms of Eq. 2, the Paris power-law exponents vary between $m \sim 35$ (at higher temperatures) and 68 (at lower temperatures). Although changing the frequency had little effect on crack-growth behavior, growth rates were accelerated with increasing temperature. ΔK_{th} thresholds are decreased from just over 5 MPa√m at 25°C to between 3.3 and 3.4 MPa√m at 1200°C, with no further decline at 1300°C. Mechanistically, the lack of a frequency effect in ABC-SiC at ambient temperatures is expected as crack advance occurs (as described above) via predominantly intergranular cracking ahead of the tip, balanced by shielding by grain bridging in the wake, both essentially rate-insensitive processes. However, the absence of a frequency effect at elevated temperatures is much more surprising, particularly since comparable materials, such as Si_3N_4, Al_2O_3 and silicide-matrix ceramics, show a marked sensitivity to frequency at temperatures above ~1000°C (see, for example, Fig. 14) due to the onset of creep damage [49,50,52,62]. As described below, fatigue fracture mechanisms at 850° to 1300°C in ABC-SiC are effectively identical to those at room temperature, which is consistent with the absence of significant creep phenomena in this microstructure below 1300°C.

It should be noted here that both the toughness and fatigue resistance of ABC-SiC are superior to commercial SiC (Hexoloy) at both room and elevated temperatures (Fig. 16). Results at 1300°C indicate that Hexoloy fails as it does as 25°C, i.e., catastrophically, with no cycle-dependent cracking, at very low stress intensities (some 40 - 50% lower than in ABC-SiC) [30,63]. Such extremely brittle behavior is attributed to the absence of toughening from crack bridging behind the crack tip, resulting from its fully transgranular mode of fracture.

A comparison of the crack-growth velocities in ABC-SiC under cyclic and static (sustained) loading is shown in Fig. 17 [63]. It can be seen that at both 25° and 1300°C, growth rates under cyclic loads were significantly faster than under sustained loading (static fatigue) at equivalent stress-intensity levels. Such behavior has been observed previously in Mg-PSZ, Al_2O_3 and Si_3N_4 [e.g.,7], and is consistent with the fact that at low temperatures, crack-advance (damage) mechanisms are identical under both types of loading; specifically, it is the cyclic-loading induced degradation in wake shielding that accelerates growth rates under cyclic loads. In contrast, the sustained-load mechanisms at elevated temperatures are generally far more damaging in such ceramics as Al_2O_3 and Si_3N_4 [e.g.,48-52] because of the onset of creep damage; however, such behavior was not seen in ABC-SiC at elevated temperatures up to 1300°C.

Fracture surfaces and crack profiles in ABC-SiC at 1300°C were for all practical purposes identical to those at ambient temperatures under both static and cyclic loads, i.e., predominantly intergranular fracture (Fig. 18a,b), with extensive interlocking grain bridging behind the crack tip (Fig. 18c,d). Also noticeable on the cyclic fatigue surfaces was the presence of debris, formed by wear and abrasion of the bridging crack faces during cycling. Clearly, the mechanisms of fatigue-crack growth in ABC-SiC, i.e.,

intergranular cracking coupled with degradation of the resulting bridging zone, are essentially identical at temperatures between 25° and 1300°C. Indeed, high-resolution transmission electron microscopy (HRTEM) studies of regions in the immediate vicinity of the crack tip provide direct confirmation of these observations; crack extension at 1300°C is predominantly along the boundaries under both sustained and cyclic loading with no indication of cavitation damage ahead of the tip or viscous-phase bridging in the wake (Fig. 18c,d). HRTEM observations also revealed that the grain-boundary films had fully crystallized (Fig. 15) *in situ* during the high-temperature fatigue tests, starting after only one hour at 1000°C. The amorphous films were found to be composed of Al-Si-O-C; on crystallization, however, they displayed a 2H-wurtzite structure with an aluminosilicate composition, i.e., a solid solution between Al_2OC and SiC.

The absence of creep damage and/or viscous softening of the grain-boundary phase at 1300°C in ABC-SiC is quite contrary to behavior reported for Si_3N_4 [50] and Al_2O_3 [49] at these temperatures, where cavitation along grain boundaries, microcracking zones, and viscous-phase bridging are commonly observed. The unique high-temperature characteristics of ABC-SiC appear to be a result of the *in situ* crystallization of grain-boundary glassy phase.

Even though the primary mechanisms of damage (intergranular cracking) and shielding (grain bridging) are apparently unchanged between 25° and 1300°C in ABC-SiC, there is a small change in the fatigue-crack growth resistance in that fatigue thresholds ΔK_{th} are approximately 30% lower at the higher temperature. This may be rationalized by considering the nature of grain bridging [42,45] and its degradation under cyclic loading due to frictional wear [38,39]. The pullout resistance from frictional tractions generated via sliding contact of opposing crack faces is proportional to the normal stress acting on the interface, which in turn is a function of the residual stress resulting from thermal expansion anisotropy during cooling from the processing temperature [45]. As the residual stresses will "anneal out" with increasing temperature, the normal stress will decrease. However, once crystallization of grain-boundary phase occurs above ~1100°C, the frictional coefficient may be expected to be higher. Thus, the minimal change in cyclic fatigue properties between 25° and 1300°C can be related to (i) the lack of any apparent change in mechanisms, (ii) the fact that the decrease in residual stress with temperature is compensated by an increase in the frictional coefficient, and (iii) the absence of significant creep damage, the latter two effects being associated with the *in situ* crystallization of the grain-boundary phase. Such a result is consistent with previous studies in other ceramics that show a beneficial effect of crystallization on oxidation and mechanical properties at elevated temperatures [65-67].

4.12.5. FATIGUE-CRACK GROWTH IN INTERMETALLIC MATERIALS

4.12.5.1. General Considerations

Like ceramics, intermetallics generally display only very restricted mobile dislocation activity at low homologous temperatures (below their brittle-to-ductile transition temperature, DBTT) due to their complex, and invariably ordered, crystal structures; consequently, they invariably have only limited ductility and toughness. To toughen intermetallics, both intrinsic and extrinsic toughening approaches have been attempted, and to varying degrees have been successful [e.g., 68-70]. For example, the intermetallic compound Nb_3Al can be toughened through the addition of a ductile phase such as Nb, with the intermetallic matrix cracking preferentially to the metallic reinforcement [71-73]. In fact, using a high-aspect ratio reinforcement, e.g., a Nb layer in an arrester laminate, the crack-initiation toughness may be enhanced *intrinsically* by the necessity of the crack in the intermetallic matrix renucleating across the metal phase. With subsequent crack extension, the uncracked Nb ligaments left in the crack wake can induce additional crack-growth (or R-curve) toughness, in this case *extrinsically* from the crack bridging created by the zone of intact ductile ligaments behind the crack tip.

In many respects, the mechanical behavior of intermetallics can be considered to be intermediate between metals and ceramics, ranging from compounds with some ductility, such as α_2-Ti_3Al, that display "metal-like" characteristics, to the very brittle Nb_3Al and $MoSi_2$ that are "ceramic-like" (below the DBTT). Specifically, with respect to fatigue-crack propagation, intrinsic damage mechanisms associated with crack advance do appear to operate in the more ductile intermetallics as in metals (although they have not been studied in detail); in contrast, the mechanism by which the crack extends in the cyclic fatigue of brittle intermetallics, such as Ni_3Al and $MoSi_2$, is identical to that occurring under monotonic loads, as in ceramics [e.g.,74,75]. Moreover, whereas the intrinsic toughening mechanisms, such as crack renucleation, do not degrade under cyclic loading, the extrinsic toughening mechanisms, such as crack bridging, can suffer severe degradation. A notable example is ductile-phase reinforced intermetallic composites, which due to extensive crack bridging by the uncracked ductile phase can display significantly higher toughness (i.e., by a factor of three or greater) than the constituent matrix [e.g., 34,71]. However, the improvement in crack-growth resistance is far less obvious in fatigue simply because the ductile phase fails prematurely; indeed, the fatigue-crack growth properties are rarely much better than that of the unreinforced matrix [34,35]. Thus, similar to ceramic materials, cyclic loading can act to reduce the potency of extrinsic toughening mechanisms in impeding crack advance.

4.12.5.2. Mechanistic Aspects

The fatigue of intermetallics has been studied far less extensively than that of metals [e.g., 76]; indeed, few microstructures or compositions have ever been optimized for maxiumum fatigue strength. The approaches that are available are to develop intrinsic toughening that will not degrade, which to date has not been too successful, or to devise extrinsic mechanisms that are more resilient to alternating loads. Below the latter approach is briefly explored, again in the context of fatigue-crack growth being a compromise between intrinsic and extrinsic processes, by examining the behavior of several intermetallic systems.

A good example of this behavior is shown by γ-TiAl alloys reinforced with small fractions of ductile Nb or TiNb, where toughening derives from tractions induced by unbroken ductile ligaments bridging the crack wake (Fig. 19) [34,35]. For small-scale bridging, the toughness increases with crack extension up to a maximum steady-state level, K_c, associated with the development of a steady-state bridging zone, and can be estimated from the flow stress σ_o, volume fraction f, and size t of the reinforcement [77]:

$$K_c = \sqrt{K_o^2 + E' f t \sigma_o \chi} \quad , \tag{16}$$

where K_o is the critical crack-tip stress intensity at crack initiation, E' is the appropriate elastic modulus of the composite, and χ is a dimensionless function representing the work of rupture. For γ-TiAl reinforced with Nb or Nb-alloys, χ varies between 0.9 and 1.5; much larger values of χ (<4) can be obtained using strain-hardening reinforcements that debond readily from the matrix [78]. For nominal values of $\chi = 1.2$, $\sigma_0 = 400$ MPa and $t = 100$ μm, the addition of a mere 20 vol.% of ductile particles yields K_c ~44 MPa√m, over five times the toughness of unreinforced TiAl [35]. Under cyclic loads, however, such bridging from unbroken ductile ligaments is compromised by the susceptibility of the ductile phase to premature fatigue failure. Accordingly, despite the factor of 3-5 increase in toughness, the fatigue-crack growth properties of the composite are comparable (and in specific orientations worse) than that of the unreinforced matrix [34,35]. However, Nb reinforcements, which undergo extensive interface debonding (due to σ-phase in the reaction layer), can delay this failure process; Nb thus provides improved fatigue resistance over reinforcements such as TiNb that is more strongly bonded to the matrix (due to an α_2-Ti_3Al reaction layer) (Fig. 19) [35].

To achieve good fatigue-crack propagation resistance in intermetallics, it is therefore necessary to develop toughening mechanisms that are more resilient to cyclic loading. For example, for ductile-phase toughened systems, several strategies are available and involve the use of:

1. *high aspect-ratio reinforcements*; this merely increases the probability of interception by the crack. For example, $MoSi_2$ reinforced with spherical Nb particles displays insignificant toughening and no improvement in fatigue resistance as the crack merely circumvents the ductile phase [74]; in contrast, with Nb wire-mesh [79] or laminate [80] reinforcements, a three-fold increases in toughness (due to extensive crack bridging) and good fatigue-crack growth resistance (due to crack closure) can be obtained.
2. *reinforcements with weakened interfaces with the matrix*; the resulting delamination at the interface acts to delay the inevitable failure of the ductile ligament, as shown by the improved fatigue properties of Nb/γ-TiAl compared to TiNb/γ-TiAl (Fig. 19) [35].
3. *reinforcements with good intrinsic fatigue resistance*; whereas β-TiNb is a useful reinforcement phase for toughening γ-TiAl because of its high strength (σ_o ~ 430 MPa), its fatigue properties are poor due to its near zero strain hardening which induces rapid shear localization. A better approach is to use monolithic γ-TiAl alloys

with lamellar microstructures, where (R-curve) toughening results from uncracked (shear) ligament bridging [81]; here, since the bridge material is the same as the matrix, there is a lower tendency for the bridges to fail preferentially in fatigue (Fig. 20) [82].

4. *reinforcements that promote other extrinsic toughening mechanisms*; since bridging mechanisms invariably fail under fatigue loading, good fatigue-crack growth resistance can be achieved if alternative shielding mechanisms develop. For example, with Nb-wire mesh reinforced $MoSi_2$, the Nb bridging ligaments which provide for R-curve toughening do fail prematurely in fatigue; however, as the crack follows the weakened interfacial reaction layer of the Nb phase, highly tortuous crack paths result which give rise to high levels of roughness-induced crack closure [79].
5. *reinforcements that promote intrinsic toughening*; whereas extrinsic shielding mechanisms tend to degrade in fatigue, intrinsic toughening mechanisms do not. Accordingly, the use of laminate reinforcements in the arrester orientation, which require the crack to renucleate across the ductile layer, both increase the crack-*initiation* toughness and remain equally potent under cyclic loading. Such behavior is shown by coarser-scale Nb/Nb_3Al laminated composites [73,83] and the newly developed boron-modified molybdenum silicide alloys [84,85] described below in section 4.12.5.2.1.

4.12.5.2.1. Intrinsic and extrinsic mechanisms

One excellent example of the use of both intrinsic and extrinsic toughening mechanisms acting *in concert* to promote some degree of resistance to fatigue-crack growth in intermetallics materials [84,85] is afforded by the recently developed boron-modified molybdenum silicide alloys [86]. Whereas $MoSi_2$-based silicides have good oxidation resistance up to 1700°C and relatively easy processibility, they are plagued, like many ordered intermetallics, by poor ductility and fracture toughness properties; in addition, they are susceptible to severe low temperature oxidation ("pesting") problems [87]. The use of higher molybdenum contents and the addition of boron, however, has led to the development of an alternative series of refractory silicide alloys, which are considerably tougher and display a much improved low-temperature "pest" resistance due to the formation of a low viscosity, passivating borosilicate glass. [86]. Many of these alloys consist either of an intermetallic matrix of Mo_3Si, and Mo_5SiB_2 (T2) phases with α-Mo precipitates (Fig. 21) or, at higher Mo contents, of a metallic α-Mo matrix with Mo_3Si, and Mo_5SiB_2 precipitates. They are significantly tougher than $MoSi_2$ largely due to the presence of the α-Mo phase [84,85].

The fracture toughness and fatigue-crack growth properties between 25° and 1300°C for one such series of alloys, of composition (in at.%) Mo 12-17Si 8.5B, are shown, respectively, in Figs. 22 and 23 [84,85]. Both the toughness and fatigue resistance can be seen to be substantially higher than that of monolithic $MoSi_2$ at ambient and elevated temperatures. Specifically, the ingot-metallurgy (I/M) alloys with the coarsest particles, highest volume fraction, and most near-continuous distribution of the α-Mo phase, show by far the best properties. In particular, the I/M Mo-12Si-8.5B alloy (IM1) displays a

relatively high intrinsic toughness at 800° up to 1200°C (~10 MPa√m) due primarily to a crack trapping toughening mechanism by α-Mo phase, with only limited extrinsic R-curve toughness. Although the lack of extrinsic toughening is not necessarily beneficial, it does imply in a brittle material that it should show a reduced susceptibility to fatigue failure, as is observed at temperatures up to 1300°C. Of particular significance though is that both the fracture toughness and the fatigue threshold are increased with increasing temperature [84]. This remarkable property is associated with the onset of additional toughening mechanisms that become active at high temperatures, specifically involving crack bridging by the α-Mo phase and microcracking primarily in the Mo_5SiB_2 phase (Fig. 26). Whereas the extrinsic crack bridging mechanism does degrade under cyclic loading due to the premature fatigue failure of the Mo particles, both the crack trapping and microcracking mechanisms appear to be equally effective under sustained and cyclic loads. Indeed, the higher Mo versions of these alloys show exceptional promise as engine materials for future propulsion systems that operate with metal temperatures well above 1000°C [84,85].

4.12.6. FATIGUE OF DUCTILE VERSUS BRITTLE MATERIALS

Compared to metallic materials where there is an extensive database and degree of understanding of fatigue failure [e.g., 1,2,88,89], ceramics and intermetallic systems still require much study with respect to developing a comprehensive understanding of their behavior under cyclic loads. In such materials, it is now clear that cyclic loading induces a progressive degradation in the toughening (or shielding) mechanisms behind the crack tip that locally elevates the near-tip driving force. It is this cyclic suppression of shielding that is considered to be the principal source for the susceptibility of brittle materials to cyclic fatigue failure. By contrast, the propagation of fatigue cracks in metallic materials involves primarily *intrinsic* damage processes occurring *ahead* of the crack tip, i.e., involving crack advance by progressive blunting and resharpening of the crack tip, clearly a mechanism distinct from fracture under monotonic loads. Additionally, shielding, in the form of crack closure (wedging) mechanisms, can act in the crack wake.

Since the physical mechanisms of crack advance and crack-tip shielding are quite different in metals and ceramics, the dependencies on the alternating and mean loads, specifically ΔK and K_{max}, the alternating and maximum stress intensities, respectively, are also quite different. A schematic illustration highlighting these differences is shown in Fig. 27 [9]. Clearly, in metals the dominant dependence of ΔK is a consequence of the intrinsic crack-advance mechanism; the smaller K_{max} dependence results primarily from its effect of the crack-opening displacement, which in turn controls the degree of crack wedging due to crack closure in the wake. Thus, for ductile metals, $n \ll p$ in Eq. 7. In ceramics, conversely, growth rates are principally a function of K_{max}, since the crack-advance mechanism is identical to that under static loading; the much weaker ΔK dependence here arises from the cyclic-induced degradation in shielding in the wake. Thus, for ceramics, $p \ll n$. In intermetallics, fatigue properties are intermediate between these two extremes, such that generally $p \sim n$. However, in brittle intermetallics such as

$MoSi_2$, where there is no intrinsic cycle-dependent crack advance mechanism, $p > n$, whereas in more ductile materials, such as the ($\gamma+\alpha_2$) TiAl alloys, intrinsic fatigue damage mechanisms, similar to those in metals, clearly exist, and $p < n$.

Such differing dependencies on ΔK and K_{max} also have a marked influence on how the load ratio affects growth rates. In metals where the ΔK term is dominant, characterizing growth rates in terms of ΔK invariably normalizes the load-ratio dependence (at least in the intermediate range of growth rates from ~10^{-9} to 10^{-6} m/cycle) [e.g., 89]. In ceramics, conversely, this normalization is achieved by characterizing growth rates as a function of K_{max} as this is the dominant term [40], whereas in intermetallics, the load ratio dependence cannot be normalized by either ΔK or K_{max} [79,82,83].

Although both intermetallics and ceramics are susceptible to fatigue-crack growth from degradation of shielding under cyclic loads, there are significant differences. At ambient temperatures, there is no intrinsic fatigue damage mechanism in ceramics - the crack tip advances by an identical mechanism under monotonic and cyclic loads; at a given stress intensity, fatigue cracks simply grow faster due to the cyclic suppression in shielding behind the crack tip. Accordingly, the value of maximum stress intensity at the fatigue threshold, $K_{max,TH}$, is comparable with the crack-initiation toughness, K_o, at the start of the R-curve ($K_{max,TH} \sim K_o$). In many intermetallics, conversely, fatigue-crack growth is seen at stress-intensity levels below the crack-initiation toughness, specifically $K_{max,TH} \sim$ 0.25-0.4 K_o, implying there are additional *intrinsic* microstructural damage mechanisms associated with fatigue failure; however, this effect is more restricted than in metals, where generally $K_{max,TH} \leq 0.1\ K_o$, due to the limited crack-tip plasticity and consequently lower toughness of intermetallic alloys.

4.12.7. FATIGUE DESIGN AND LIFE PREDICTION

The use of standard damage-tolerant design and life-prediction methods for structural components fabricated from ceramics and intermetallics is complicated by the marked sensitivity of their fatigue-crack growth rates to the applied stress intensity both at elevated and especially ambient temperatures. For safety-critical applications involving most metallic structures, such procedures generally rely on the integration of data relating crack-growth rates (*da/dN* or *da/dt*) to the applied stress intensity (ΔK or K_{max}) in order to estimate the time or number of cycles, N_f, to grow the largest undetectable initial flaw, a_i, to critical size a_c, viz:

$$N_f = \frac{2}{(m-2)\,C\,(Q\,\Delta\sigma)^m\ \pi^{m/2}}\left[a_o^{(2-m)/2} - a_c^{(2-m)/2}\right] \qquad (17)$$

where $\Delta\sigma$ is the applied stress range, Q is the geometric factor; C and m ($\neq 2$) are the scaling constant and exponent in the crack-growth relationship in Eq. 2. For advanced materials such as intermetallics and ceramics, this approach may be difficult to implement in practice due to the large values of the exponent m; since the projected life is proportional to the reciprocal of the applied stress raised to the power of m, a factor of

two change in applied stress can lead to projections of the life of a ceramic component (where m can be as high as 20 or more) to vary by more than six orders of magnitude. Essentially, because of the high exponents, the life spent in crack propagation in advanced materials will be extremely limited or infinitely large, depending upon whether the initial stress intensity is above or below the fatigue threshold.

Accordingly, a more appropriate approach may be to design on the basis of a threshold below which fatigue failure cannot occur; this may involve a conventional fatigue-crack initiation threshold or fatigue limit determined from stress-life (*S/N*) data or, more conservatively, the ΔK_{TH} or $K_{max,TH}$ thresholds for no crack growth. However, even these approaches may not be conservative due to uncertainties in the definition of such thresholds. This is particularly important in many advanced materials as their growth-rate curves are not sigmoidal and correspondingly show little evidence of a threshold. Moreover, as with metallic materials [e.g., 90,91], there is now increasing evidence for small-crack effects in both ceramics [29,32] and intermetallics [92], where cracks of a size comparable with the scale of microstructure, the extent of local inelasticity ahead of the crack tip, or with the extent of shielding in the wake of the tip, can propagate at applied stress intensities *below* the "long-crack" ΔK_{TH} or $K_{max,TH}$ thresholds. Clearly for flaw-sensitive materials such as ceramics and intermetallics to be safely used in fatigue-critical applications, the critical levels of damage necessary for the *onset* of fatigue failure must be defined; whether this involves an *S/N* fatigue limit, large- or small-crack thresholds, or probabilistic analyses is as yet still unclear.

4.12.8 SUMMARY AND CONCLUSIONS

Over the past few decades, there have been major advances in the design and development of brittle solids as structural materials, despite their still limited use for most structural applications. This has primarily been achieved by developing ceramics and intermetallics with significantly improved fracture resistance, principally through the use of the extrinsic shielding approach to toughening. This has included the design of microstructures which develop zones of inelasticity, microcracking or most predominantly bridging (by grains, particulate, fibers or layers) that surround the crack. However, it is now evident that cyclic fatigue loading can severely degrade such toughening; in fact, this provides the critical mechanism promoting fatigue-crack growth, even in materials such as ceramics that display no intrinsic mechanism of cyclic crack advance.

Although the mechanisms of cyclic fatigue in brittle materials are conceptually different from the well known mechanisms of metal fatigue, the central thesis of this chapter is that by considering the relative importance of the prevailing intrinsic damage and extrinsic shielding mechanisms, a commonality of behavior can be found for the cyclic fatigue of both ductile and brittle materials. However, as noted above, the respective contributions of each mechanism does result in marked differences in the ΔK and K_{max} dependence of growth rates, the load ratio effect and the relationship of the fatigue threshold to the toughness properties; these are summarized in Table I.

Table I.
Differences in the Fatigue-Crack Growth Properties of Ductile and Brittle Materials

	$da/dN \propto (K_{max})^n(\Delta K)^p$	relationship of $K_{max,TH}$ to K_o*
Metals	$p >> n$	$K_{max,TH} \leq 0.1\ K_o$
Intermetallics	$p \sim n$	$K_{max,TH} \sim 0.25\text{-}0.4\ K_o$
Ceramics	$p << n$	$K_{max,TH} \sim K_o$

* $K_{max,TH}$ and K_o are, respectively, the fatigue threshold and the crack-initiation toughness on the R-curve.

Finally, the marked sensitivity of growth rates to the applied stress intensity in ceramics and intermetallics implies that projected lifetimes will be a very strong function of stress and crack size; this makes design and life prediction using damage-tolerant methodologies more complex. Accordingly, design approaches based on the definition of a critical level of damage for the *onset* of fatigue cracking must be contemplated, involving either an *S-N* fatigue limit or crack-propagation threshold, provided due attention is given to the fact that these approaches may not be conservative due to the sub-threshold extension of small cracks.

4.12.9. ACKNOWLEDGMENTS

This work was supported by the Director, Office of Energy Research, Office of Basic Energy Sciences, Division of Materials Sciences and Engineering, of the U.S. Department of Energy under Contract No. DE-AC03-76SF00098 (for studies on ceramics) and Air Force Office of Scientific Research under Grant No. F49620-96-1-0223 and F49620-97-1-0365 (metals and intermetallics). Thanks are due to Dr. L. C. DeJonghe and X.-F. Zhang and to past and present members of my research group, in particular Drs. B. L. Boyce, D. R. Bloyer, J. P. Campbell, Da Chen, H. Choe, R. H. Dauskardt, C. J. Gilbert, J. J. Kruzic, A. L. McKelvey, J. M. McNaney, R. K. Nalla, V. Schroeder, and K. T. Venkateswara Rao, whose research forms the major basis for this manuscript.

4.12.10. REFERENCES

1. S. Suresh, *Fatigue of Materials*, Cambridge University Press, Cambridge (1991).
2. F. Ellyin, *Fatigue Damage, Crack Growth and Life Prediction*, Chapman & Hall, London (1997).
3. G. F. Harrison and M. R. Winstone, "Aeroengine Applications of Advanced High Temperature Materials," in *Mechanical Behaviour of Materials at High Temperatures*, C. Moura Branco, R. O. Ritchie and V. Sklenicka, eds., Kluwer Academic, Dordrecht, The Netherlands (1996) 309-325.

4. R. Kochendörfer, "CMC Processing Routes for High Temperature Applications," in *Mechanical Behaviour of Materials at High Temperatures*, C. Moura Branco, R. O. Ritchie and V. Sklenicka, eds., Kluwer Academic, Dordrecht, The Netherlands (1996) 635-682.
5. R. O. Ritchie, "Fatigue and Fracture of Pyrolytic Carbon: A Damage-Tolerant Approach to Structural Integrity and Life Prediction in "Ceramic" Heart-Valve Prostheses," *J. Heart Valve Disease* 5, suppl. 1 (1996) S9-31.
6. R. H. Dauskardt, W. Yu, and R. O. Ritchie, "Fatigue Crack Propagation in Transformation-Toughened Zirconia Ceramic," *J. Am. Ceram. Soc*. 70 (1987) C248-252.
7. R. O. Ritchie and R. H. Dauskardt, "Cyclic Fatigue of Ceramics: A Fracture Mechanics Approach to Subcritical Crack Growth and Life Prediction," *J. Ceram. Soc. Japan* 99 (1991) 1047-1062.
8. R. O. Ritchie, "Mechanisms of Fatigue Crack Propagation in Metals, Ceramics and Composites: Role of Crack-Tip Shielding," *Mater. Sci. Eng*. A103 (1988) 15-28.
9. R. O. Ritchie, "Mechanisms of Fatigue-Crack Propagation in Ductile and Brittle Solids," *Int. J. Fract.* 100 (1999) 55-83.
10. R. M. N. Pelloux, "Mechanisms of Formation of Ductile Fatigue Striations," *Trans. ASM* 62 (1969) 281-285.
11. P. Neumann, "Coarse Slip Model in Fatigue," *Acta Metall*. 17 (1969) 1219-1225.
12. A. G. Evans, "Perspective on the Development of High Toughness Ceramics," *J. Am. Ceram. Soc*. 73 (1990) 187-206.
13. P. Becher, "Microstructural Design of Toughened Ceramics," *J. Am. Ceram. Soc*. 74 (1991) 255-269.
14. A. Wöhler, "Versuche Über die Festiykeit Eisenbahnwagenuchsen," *Zeitschrift für Bauwesen* 10 (1860).
15. H. H. Johnson and P. C. Paris, "Subcritical Flaw Growth," *Eng. Fract. Mech*. 1 (1967) 3.
16. P. C. Paris and F. Erdogan, "A Critical Analysis of Crack Propagation Laws," *J. Basic. Eng.,* Trans. ASME, Ser. D 85 (1963) 528-534.
17. R. O. Ritchie, "Influence of Microstructure on Near-Threshold Fatigue Crack Propagation in Ultra-High Strength Steel," *Metal Science* 11 (1977) 368-381.
18. N. E. Dowling and J. A. Begley, "Fatigue Crack Growth During Gross Plasticity and the J-intetral," in *Mechanics of Crack Growth*, ASTM STP 590, Am. Soc. Test. Matls., Philadelphia (1976) 82-103.
19. C. Laird and G. C. Smith, "Crack Propagation in High Stress Fatigue," *Philos. Mag*. 8 (1962) 847-857.
20. F. A. McClintock, "Discussion to C. Laird's paper 'The Influence of Metallurgical Microstructure on the Mechanisms of Fatigue Crack Propagation'," in *Fatigue Crack Propagation*, ASTM STP 415, Am. Soc. Test. Matls., Philadelphia, (1967) 170-174.
21. C. J. Gilbert, V. Schroeder, and R. O. Ritchie, W. L. Johnson, "Mechanisms for Fracture and Fatigue-Crack Propagation in a Bulk Metallic Glass," *Metall. Mater. Trans. A* 30A (1999) 1739-1753.
22. R. O. Ritchie and J. F. Knott, "Mechanisms of Fatigue Crack Growth in Low Alloy Steel," *Acta Metall*. 21 (1973) 639-650.

23. G. R. Yoder, Y. A. Cooley, and T. W. Crooker, "Quantitative Analysis of Microstructural Effects on Fatigue Crack Growth in Widmanstätten Ti-6Al-4V and Ti-8Al-1Mo-1V," *Eng. Fract. Mech*. 11 (1979) 805-816.
24. W. Elber, "Fatigue Crack Closure under Cyclic Tension," *Eng. Fract. Mech*. 2 (1970) 37-45.
25. S. Suresh and R. O. Ritchie, "Near-Threshold Fatigue Crack Propagation: A Perspective on the Role of Crack Closure," in *Fatigue Crack Growth Threshold Concepts*, D. L. Davidson and S. Suresh, eds., TMS-AIME, Warrendale (1984) 227-261.
26. A. G. Evans and E. R. Fuller, "Crack Propagation in Ceramic Materials under Cyclic Loading Conditions," *Metall. Trans. A* 5A (1974) 27.
27. S. J. Dill, S. J. Bennison, and R. H. Dauskardt, "Subcritical Crack-Growth Behavior of Borosilicate Glass under Cyclic Loads: Evidence of a Mechanical Fatigue Effect," *J. Am. Ceram. Soc*. 80 (1997) 773-776.
28. C. L. Muhlstein, E. A. Stach, and R. O. Ritchie, "Mechanisms of Fatigue in Micron-Scale Films of Polycrystalline Silicon for Microelectromechanical Systems", *Appl. Phys. Lett*., 80 (2002) 1532-1534.
29. A. A. Steffen, R. H. Dauskardt, and R. O. Ritchie, "Cyclic Fatigue Life and Crack-Growth Behavior of Microstructurally-Small Cracks in Magnesia-Partially-Stabilized Zirconia Ceramics," *J. Am. Ceram. Soc*. 74 (1991) 1259-1268.
30. D. Chen, C. J. Gilbert, X. F. Shang, and R. O. Ritchie, "High-Temperature Cyclic Fatigue-Crack Growth Behavior in an *In Situ* Toughened Silicon Carbide", *Acta Mater*. 48 (2000) 659-674.
31. S.-Y. Liu and I.-W. Chen, "Fatigue of Yttria-Stabilized Zirconia. I. Fatigue Damage, Fracture Origins, and Lifetime Prediction," *J. Am. Ceram. Soc*. 74 (1991) 1197-1205.
32. R. H. Dauskardt, M. R. James, J. R. Porter, and R. O. Ritchie, "Cyclic Fatigue-Crack Growth in SiC-Whisker-Reinforced Alumina Ceramic Composite: Long and Small-Crack Behavior," *J. Am. Ceram. Soc*. 75 (1992) 759-771.
33. R. H. Van Stone, "Residual Life Prediction Methods for Gas Turbine Components," *Mater. Sci. Eng*. A103 (1988) 49-61
34. K. T. Venkateswara Rao, G. R. Odette, and R.O. Ritchie, "On the Contrasting Role of Ductile-Phase Reinforcements in the Fracture Toughness and Fatigue-Crack Propagation Resistance of TiNb/γ-TiAl Intermetallic-Matrix Composites," *Acta. Metall. Mater*. 40 (1992) 353-361.
35. K. T. Venkateswara Rao, G. R. Odette, and R.O. Ritchie, "Ductile-Reinforcement Toughening in γ-TiAl Intermetallic-Matrix Composites under Monotonic and Cyclic Loading: Effect on Fracture Toughness and Fatigue-Crack Propagation Resistance," *Acta. Metall. Mater*. 42 (1994) 893-911.
36. D. Rouby and P. Reynaud, "Fatigue Behavior Related to Interface Modification during Load Cycling in Ceramic-Matrix Reinforced Composites," *Comp. Sci. Technol*. 48 (1993) 109-118.
37. S. Lathabai, J. Rödel, and B. R. Lawn, "Cyclic Fatigue Behavior of an Alumina Ceramic with Crack-Resistance Characteristics," *J. Am. Ceram. Soc*. 74 (1991) 1340-1348.

38. R. H. Dauskardt,"A Frictional-Wear Mechanism for Fatigue-Crack Growth in Grain Bridging Ceramics," *Acta Metall. Mater*. 41 (1993) 2765-2781.
39. H. Kishimoto, A. Ueno, and H. Kawamoto, "Crack Propagation Behavior and Mechanism of a Sintered Silicon Nitride under Cyclic Load," in *Cyclic Fatigue in Ceramics*, H. Kishimoto, T. Hoshide, and N. Okabe, eds., Elsevier, London (1995) 101-122.
40. C. J. Gilbert, J. J. Cao, W. J. MoberlyChan, L. C. DeJonghe, and R. O. Ritchie, "Cyclic Fatigue and Resistance-Curve Behavior of an *In Situ* Toughened Silicon Carbide with Al-B-C Additions," *Acta Mater*. 44 (1996) 3199-3214.
41. C. J. Gilbert, and R. O. Ritchie, "On the Quantification of Bridging Tractions during Subcritical Crack Growth under Monotonic and Cyclic Fatigue Loading in a Grain-Bridging Silicon Carbide Ceramic," *Acta Mater*. 46 (1998) 609-616.
42. B. R. Lawn, *Fracture of Brittle Solids*, 2nd ed., Cambridge University Press, Cambridge (1993).
43. J. C. Hay and K. W. White, "Grain-Bridging Mechanisms in Monolithic Alumina and Spinel," *J. Am. Ceram. Soc*. 76 (1993) 1849-1854.
44. Y.-W. Mai and B. R. Lawn, "Crack-Interface Grain Bridging as a Fracture Resistance Mechanism in Ceramics. II. Theoretical Fracture Mechanics Model," *J. Am. Ceram. Soc*. 70 (1987) 289-294.
45. R. M. L. Foote, Y.-W. Mai, and B. Cotterell, "Crack Growth Resistance Curves in Strain-Softening Materials," *J. Mech. Phys. Solids* 34 (1986) 593-607.
46. G. I. Barenblatt, "The Mathematical Theory of Equilibrium Cracks in Brittle Fracture," *Adv. Appl. Mech*. 7 (1962) 55-129.
47. G. R. Irwin, "Fracture," in *Handbuch der Physik*, Springer-Verlag, Berlin, Germany, 6 (1958) 551.
48. L. X. Han and S. Suresh, "High-temperature Failure of an Alumina-Silicon Carbide Composite under Cyclic Loads: Mechanisms of Fatigue Crack-Tip Damage", *J. Am. Ceram. Soc*., 72 (1989) 1233-1238.
49. L. Ewart and S. Suresh, "Elevated-temperature Crack Growth in Polycrystalline Alumina under Static and Cyclic Loads", *J. Mater. Sci.* 27 (1992), 5181-5191.
50. U. Ramamurty, T. Hansson, and S. Suresh, S., High-Temperature Crack Growth in Monolithic and SiC_w-Reinforced Silicon Nitride under Static and Cyclic Loads", *J. Am. Ceram. Soc*., 77 (1994), 2985-99.
51. H. Kishimoto, A. Ueno, H. Kawamoto, and A. Tomitaka, "Crack Propagation Behavior of Sintered Silicon Nitride under Cyclic Load at Elevated Temperature (Effect of Stress Ratio)" *J. Soc. Mater. Sci., Japan* 41 (1992), 1805-1810.
52. A. Ueno, H. Kishimoto, H. Kawamoto, and T. Murasawa, "Crack Propagation Behavior of Sintered Silicon Nitride under Cyclic Load at Elevated Temperature (Influences of Frequency and Stress Wave Form)" *J. Soc. Mater. Sci., Japan* 42 (1993), 976-982.
53. C.-H. Huang and J.-K., Shang, "Shear-Driven High-Temperature Fatigue Crack Growth in Polycrystalline Alumina *Acta Metall. Mater.* 43 (1995), 4179-4187.
54. S.-Y. Liu and I.-W. Chen, "High Temperature Crack Growth in Silicon Nitride under Static and Cyclic Loading: Short-Crack Behavior and Brittle-Ductile Transition", *Acta Mater*. 44 (1996), 2079-2092.

55. A. Ziegler, J. M. McNaney, andR. O. Ritchie, "Subcritical Crack Growth in NT-164 Silicon Nitride at Elevated Temperatures. in *Proc. 9th CIMTEC-World Ceramics Congress and Forum on New Materials* (Florence, Italy, June 14-19, 1998), P. Vincenzini, ed.
56. Y. H. Zhang and L. Edwards, "Cyclic Fatigue Crack Growth Behaviour of Silicon Nitride at 1400°C", *Mater. Sci. Eng*., 256A (1998) 144-151.
57. D. S. Wilkinson and V. Vitek, "The Propagation of Cracks by Cavitation: A General Theory", *Acta Metall.* 30 (1982), 1723-1732.
58. N. Dey, D. F. Socie, and K. J. Hsia, "Modeling Static and Cyclic Fatigue in Ceramics Containing a Viscous Grain Boundary Phase", *Acta Metall. Mater*. 43 (1995), 2163-2175.
59. U. Ramamurty, "Retardation of Fatigue Crack Growth in Ceramics by Glassy Ligaments: A Rationalization. *J. Am. Ceram. Soc*., 79 (1996), 945-952.
60. K. S. Yi, B. N. Cox, and R. H. Dauskardt, "Fatigue Crack-Growth Behavior of Materials in Viscous Fluid Environments", *J. Mech. Phys. Sol*., 47 (1999) 1843-1871.
61. J. M. McNaney, C. J. Gilbert, and R. O. Ritchie, "Effect of Viscous Grain Bridging on Cyclic Fatigue-Crack Growth in Monolithic Ceramics at Elevated Temperatures", *Acta Mater.* 47 (1999) 2809-2819.
62. Y. Miyashita, H. Maruta, T. Hansson, S. Zhu, and Y. Mutoh, "Micromechanism of High Temperature Fatigue Crack Growth in Silicon Nitride", *J. Soc. Mater. Sci., Japan* 47 (1998), 899-904.
63. D. Chen, M. F. Sixta, X. F. Zhang, L. C. De Jonghe, and R. O. Ritchie, "Role of the Grain-Boundary Phase on the Elevated-Temperature Strength, Toughness, Fatigue and Creep Resistance of Silicon Carbide Sintered with Al. B and C", *Acta Mater.* 48 (2000) 4599-4608.
64. D. Chen, C. J. Gilbert, X. F. Zhang, and R. O. Ritchie, "Effects of Grain-Boundary Structure on the Strength, Toughness and Cyclic Fatigue Properties of a Monolithic Silicon Carbide", *J. Am. Ceram. Soc*.,, 85 (2000) 2079-2081.
65. F. F. Lange, B. I. Davis, and M. G. Metcalf, "Strengthening of Polyphase Si_3N_4 Materials Through Oxidation" *J. Mater. Sci*., 18 (1983) 1497-1505.
66. M. K. Cinibulk, G. Thomas, and S. M. Johnson, "Grain-Boundary-Phase Crystallization and Strength of Silicon Nitride Sintered with a YSiAlON glass" *J. Am. Ceram. Soc.*, 73 (1990) 1606-1612.
67. M. K. Cinibulk, G. Thomas, and S. M. Johnson, "Strength and Creep Behavior of Rare-Earth Disilicate-Silicon Nitride Ceramics" *J. Am. Ceram. Soc.*, 75 (1992) 2050-2055.
68. C. T. Liu, A. I. Taub, N. S. Stoloff, and C. C. Koch, eds., *High-Temperature Ordered Intermetallic Alloys III*, MRS Symp. Proc., 133, Materials Research Society, Pittsburgh (1989).
69. D. P. Pope, C. T. Liu, and S. H. Whang, eds., *High Temperature Intermetallics - Parts 1 & 2*, Elsevier, Lausanne, Switzerland (1995).
70. W. O. Soboyejo, T. S. Srivatsan, and R. O. Ritchie, eds., *Fatigue and Fracture of Ordered Intermetallic Materials II*, TMS, Warrendale (1995).
71. L. Murugesh, K. T. Venkateswara Rao, and R. O. Ritchie, "Crack Growth in a Ductile-Phase-Toughened Nb/Nb_3Al *In Situ* Intermetallic Composite under Monotonic and Cyclic Loading," *Scripta Metall. Mater*. 29 (1993) 1107-1112.

72. H. C. Cao, J. P. Löfvander, A. G. Evans, R. G. Rowe, and D. W. Skelly, "Mechanical Properties of an *In Situ* Synthesized Nb/Nb_3Al Layered Composite," *Mater. Sci. Eng.* A185 (1994) 87-95.
73. D. R. Bloyer, K. T. Venkateswara Rao, and R. O. Ritchie, "Fracture Toughness and R-Curve Behavior of Laminated Brittle-Matrix Composites," *Metall. Mater. Trans. A* 29A (1998) 2483-2496.
74. K. T. Venkateswara Rao, W. O. Soboyejo, and R. O. Ritchie, "Ductile-Phase Toughening and Fatigue-Crack Growth in Nb-Reinforced Molybdenum Disilicide Intermetallic Composites," *Metall. Trans. A* 23 (1992) 2249-2257.
75. M.-H. Hong, J, M. McNaney, and R. O. Ritchie, "Fatigue-Crack Growth of Small Cracks in a Directionally-Solidified Nickel Aluminide with Molybdenum Additions," *Scripta Mater.* 38 (1998) 245-251.
76. N. S. Stoloff, "Fatigue and Fracture of High Temperature Intermetallics," in *Processing and Design Issues in High-Temperature Materials*, N. S. Stoloff and R. H. Jones, eds., TMS, Warrendale (1996) 195-207.
77. M. F. Ashby, F. J. Blunt, and M. Bannister, "Flow Characteristics of Highly Constrained Metal Wires," *Acta Metall*. 37 (1989) 1847-1857.
78. H. E. Dève, A. G. Evans, G. R. Odette, R. Mehrabian, M. L. Emiliani and R. J. Hecht, "Ductile Reinforcement Toughening of γ-TiAl: Effects of Debonding and Ductility," *Acta Metall. Mater*. 38 (1990) 1491-1502.
79. K. Badrinarayanan, A. L. McKelvey, K. T. Venkateswara Rao, and R. O. Ritchie, "Fracture and Fatigue-Crack Growth in Ductile-Phase Toughened Molybdenum Disilicide: Effects of Niobium Wire vs. Particulate Reinforcements," *Metall. Mater. Trans. A* 27 (1996) 3781-3792.
80. W. O. Soboyejo, F. Ye, L.-C. Chen, N. Bahtishi, D. S. Schwartz, and R. J. Lederich, "Effects of Reinforcement Architecture on the Fatigue and Fracture Behavior of $MoSi_2$/Nb Composites," in *Fatigue and Fracture of Ordered Intermetallic Materials II*, W. O. Soboyejo, T. S. Srivatsan, and R. O. Ritchie, eds., TMS, Warrendale (1995) 359-390.
81. K. S. Chan, "Evidence of Shear Ligament Toughening in TiAl-Base Alloys," *Metall. Mater. Trans. A* 26 (1995) 1407-1418.
82. J. P. Campbell, K. T. Venkateswara Rao, and R. O. Ritchie, "The Effect of Microstructure on Fracture Toughness and Fatigue-Crack Growth Behavior in γ-Titanium Aluminide Based Intermetallics," *Metall. Mater. Trans. A* 30A (1998) 563-577.
83. D. R. Bloyer, K. T. Venkateswara Rao, and R. O. Ritchie, "Fatigue-Crack Propagation Behavior of Ductile/Brittle Laminated Composites," *Metall. Mater. Trans. A* 30A (1999) 563-577.
84. H. Choe, D. Chen, J. H. Schneibel, and R. O. Ritchie, "Ambient to High Temperature Fracture Toughness and Fatigue-Crack Propagation in a Mo-12Si-8.5B (at.%) Intermetallic", *Intermetallics* 9 (2001) 319-329.
85. H. Choe, D. Chen, J. H. Schneibel, and R. O. Ritchie, "Fracture and Fatigue Properties of Mo-Mo_3Si-Mo_5SiB_2 Refractory Intermetallic Alloys at Ambient to Elevated Temperatures (25° – 1300°C)", *Metall. Mater. Trans. A,* (2002) in review.
86. D. M. Berczik, U.S. Patent No. 5, 595, 616 and No. 5, 693, 156, United Technologies Corp., East Hartford, CT (1997).

87. M. K. Meyer and M. Akinc, “Isothermal Oxidation Behavior of Mo-Si-B Intermetallics at 1450°C”, *J. Am. Ceram. Soc*. 79 (1966) 2763-2766.
88. D. L. Davidson and J. Lankford, “Fatigue Crack Growth in Metals and Alloys: Mechanisms and Micromechanics," *Int. Mater. Reviews* 37 (1992) 45-76.
89. R. O. Ritchie, “Near-Threshold Fatigue Crack Propagation in Steels,” *Int. Metals Reviews* 20 (1979) 205-230.
90. R. O. Ritchie and J. Lankford, eds., *Small Fatigue Cracks*, TMS-AIME, Warrendale, (1986).
91. K. J. Miller and E. R. de los Rios, eds., *Short Fatigue Cracks*, Mech. Eng. Publ. Ltd., London (1992).
92. J. J. Kruzic, J. P. Campbell, and R. O. Ritchie, “On the Fatigue Behavior of γ-Based Titanium Aluminides: Role of Small Cracks,” *Acta Mater.*, 47 (1999) 801-816.

LIST OF FIGURES

Figure 9: Crack-tip shielding from bridging by interlocking grains (inset) showing (b) the variation in bridging tractions $p(X)$ due to debonding and frictional pullout, and the corresponding crack-opening profile, as a function of the crack opening displacement ($2u$) [42]. Under cyclic loading, the bridging is observed to decay, i.e., *p(u)* is progressively decreased.

Figure 10. Measured crack-opening profiles in an ABC-SiC ceramic for (a) where the crack was grown near instability (on the R-curve), and where the crack was grown by fatigue near threshold (at ~1 x 10^{-10} m/cycle at ~75% K_c). In (b), the best-fit bridging traction distributions are plotted for each case [41].

Figure 11: Model for crack-tip shielding at higher temperatures from viscous grain-boundary film bridging, showing the development of the viscous force resulting from the velocity gradient in the film [61].

Figure 12: Self-consistent solution results showing predicted variations in the maximum, K_{max}, and minimum, K_{min}, crack-tip stress intensity, normalized to the maximum applied stress intensity, K^{∞}_{max}, versus changes in the model parameters, namely (a) grain aspect ratio, d/h, (b) viscosity, η, and (c) frequency, f. The normalized crack-tip stress intensity range, $\Delta K / K^{\infty}_{max}$, is shown as the difference between the two curves [61].

Figure 13: Self-consistent solution results showing variations the crack-tip stress-intensity range, ΔK, normalized by the applied stress-intensity range, ΔK_a, versus the non-dimensional parameter Γ. Changes in the individual parameters of the model are shown by symbols while the parabolic solution is denoted by the solid line. Note that the self-consistent solution, which diverges from the parabolic at high Γ, is well-represented over the entire range by Γ [61].

Figure 14: Effect of cyclic frequency (2-20 Hz) on cyclic fatigue-crack growth rates, as a function of K_{max}, in gas-pressure sintered silicon nitride (EC-14) at 1200° and 1300°C, as compared to 20 Hz data at room temperature [62].

Figure 15. High-resolution transmission electron micrographs of the grain boundaries in ABC-SiC in the (a) as-processed, and (b) thermally exposed (1300°C for ~ 72 hr) conditions. Note the complete crystallization of the amorphous phase after exposure compared to the glass film of ~ 1 nm under as-processed condition [30].

Figure 16. Cyclic fatigue-crack growth rates, da/dN, in ABC-SiC as a function of the applied stress-intensity range ΔK for the tests conducted at temperatures between 25 and 1300°C, load ratio R = 0.1, and frequencies between 3 and

1000 Hz. For comparison, the crack growth behavior of commercial SiC (Hexoloy) is also illustrated [30,63].

Figure 17. Crack extension, Δa, plotted as function of time, t, in ABC-SiC demonstrating the effect of sustained loading vs. cyclic loading conditions, at a fixed maximum stress intensity ($K_I = K_{max}$). Plotted is behavior at 25°C, where $K_I = K_{max} = 5.9$ MPa$\sqrt{m}$, and at 1300°C, where $K_I = K_{max} = 4.1$ MPa$\sqrt{m}$ [30,63].

Figure 18. Comparison of crack growth under sustained (static) and cyclic fatigue loading ABC-SiC at elevated temperatures (1300°C), showing scanning electron micrographs of the fracture surfaces under (a) sustained and (b) cyclic loads, and transmission electron micrographs of the crack profiles at the crack-tip region in under (c) sustained loading ($K_I = 4.1$ MPa$\sqrt{m}$) and (d) cyclic fatigue loading ($R = 0.1$, $\nu = 25$ Hz, $K_{max} = 4.1$ MPa$\sqrt{m}$). Arrows indicate the general direction of crack propagation [30].

Figure 19. (a) Fracture toughness and (b) fatigue-crack growth behavior in a 20 vol.% TiNb-reinforced γ-TiAl intermetallic composite at 25°C at $R = 0.1$ in the edge (C-R) and face (C-L) orientations, where the results are compared to data for pure γ-TiAl, β-TiNb and a Nb-particulate reinforced γ-TiAl composite. (c) Extensive crack bridging by the uncracked ductile phase under monotonic loading is severely degraded under cyclic loading due to (d) premature fatigue failure of the ductile ligaments [34,35].

Figure 20. (a) Crack-tip shielding by uncracked (shear) ligament bridging in ($\gamma+\alpha_2$) titanium aluminide (e.g., Ti-47wt.%Al) alloys promotes excellent (b) R-curve toughening and (c) fatigue-crack growth resistance (compared to single-phase γ), particularly in the coarser lamellar microstructures. Such bridging does degrade under cyclic loading; however, the uncracked ligaments do not necessarily fail preferentially (as in ductile-phase bridging) as they are the same material as the matrix [82].

Figure 21. Scanning electron micrograph of the microstructure in the I/M Mo-12Si-8.5B (at.%) refractory silicide alloy, showing coarse α-Mo particles in an intermetallic matrix of Mo_3Si and Mo_5SiB_2 (T2) phases. (Etchant: Murakami's reagent) [84].

Figure 22. Fracture toughness in the form of R-curve behavior for a series of I/M and P/M Mo-Si-B alloys, showing crack-growth resistance, K_R, plotted as a function of crack extension, Δa, for the I/M and P/M alloys between 25° and 1300°C. IM1 and IM2 are I/M alloys with composition (at.%) Mo-12Si-8.5B and Mo-12Si-10Nb-8.5B, respectively; PM1 and PM2 are P/M alloys both with composition (at.%) Mo-16.8Si-8.4B. Results for the boron-modified molybdenum silicides are compared with previous data [74] on monolithic and Nb-particulate reinforced $MoSi_2$ [84,85].

Figure 23. Variation in cyclic fatigue-crack propagation rates, d*a*/d*N*, as a function of the applied maximum, K_{max}, and alternating, ΔK, stress intensities, in the same series of boron-modified molybdenum silicide alloys shown in Figure 22, at a load ratio *R* of 0.1 between 25° and 1300°C [84,85]. Shown for comparison are previous results [74] for Nb-particulate reinforced $MoSi_2$.

Figure 24. The interaction of crack path with the microstructure in an I/M Mo-12Si-8.5B alloy (IM1). In (a), crack arrest occurs at a large (~ 30 μm) α-Mo particle at 25°C; whereas the main crack readily propagates through, or around, the smaller Mo particles, the larger particles act as significant crack traps. In (b), extensive microcracking, primarily in the Mo_5SiB_2 phase, is seen parallel to the main crack at 1300°C. Horizontal arrow represents direction of crack growth [84,85].

Figure 25. Schematic illustrations of the intrinsic and extrinsic mechanisms involved in cyclic fatigue-crack growth in (a) metals and (b) ceramics, showing the relative dependencies of growth rates, *da*/*dN*, on the alternating, ΔK, and maximum K_{max}, stress intensities [9].

FIGURES

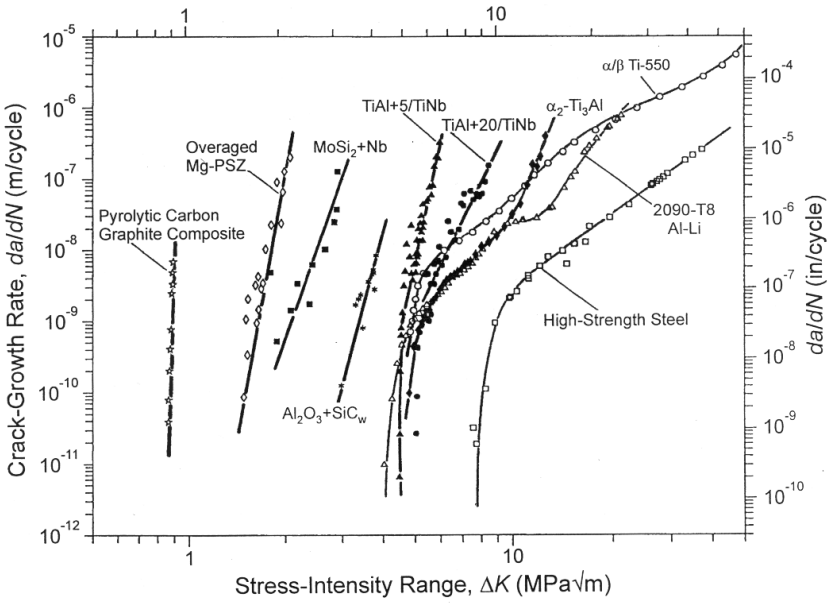

Fig. 1: Schematic variation of fatigue-crack propagation rate (da/dN) with applied stress intensity range (ΔK), for metals, intermetallics and ceramics.

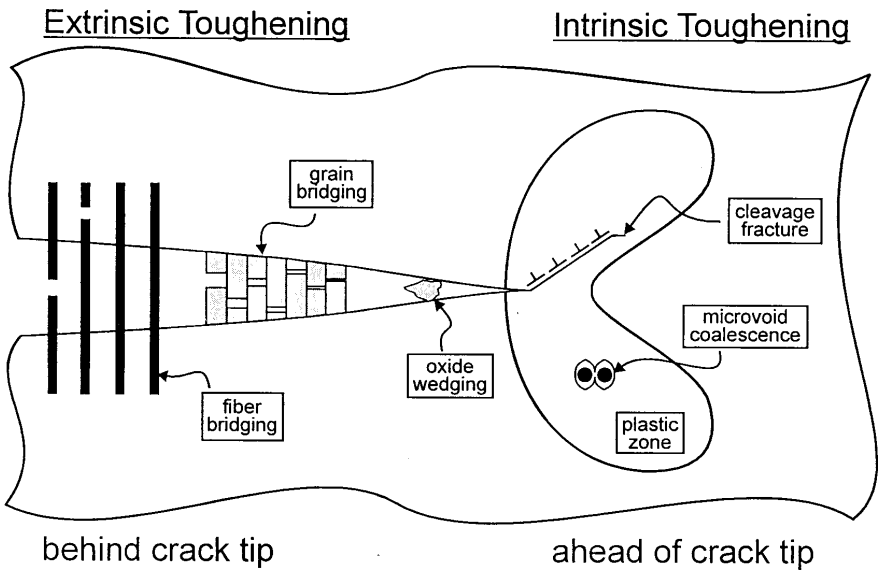

Fig. 2: Schematic illustration of mutual competition between intrinsic mechanisms of damage/crack advance and extrinsic mechanisms of crack-tip shielding involved in crack growth.

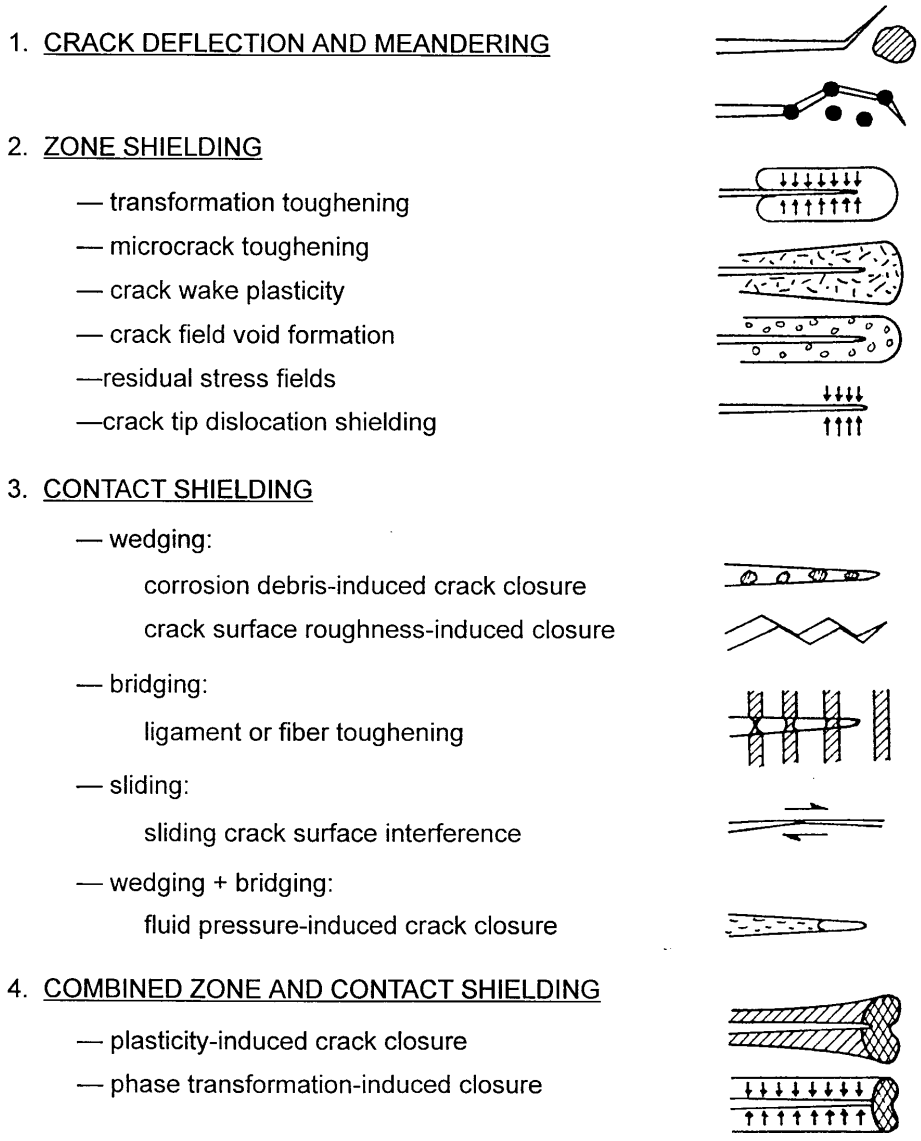

Fig. 3: Schematic illustration of the mechanisms of extrinsic toughening, involving crack deflection and crack-tip shielding by inelastic zone or contact between the crack surfaces [8].

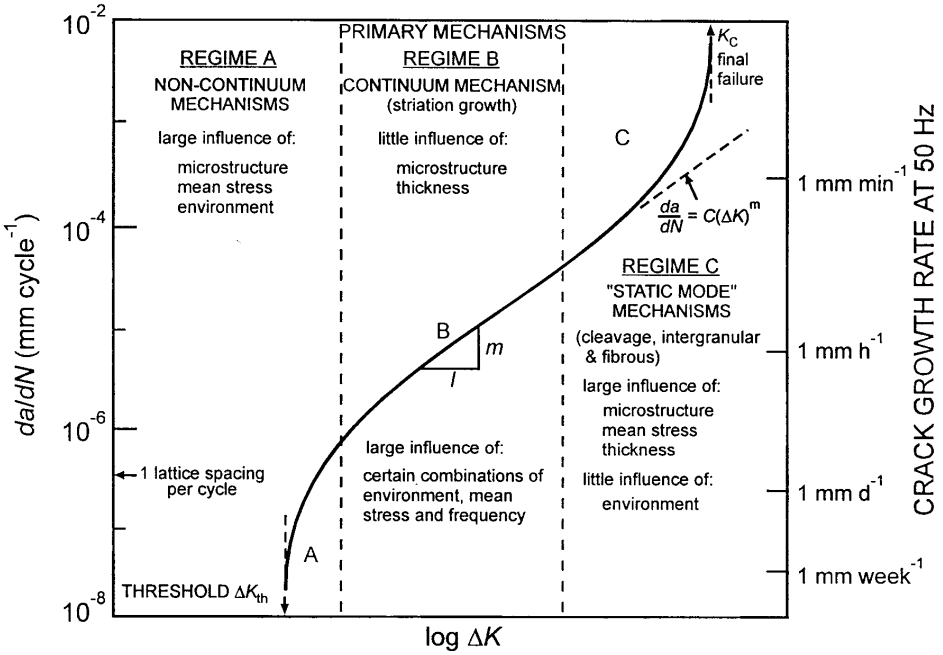

Fig. 4: Schematic illustration of the typical variation in fatigue-crack growth rates, *da*/*dN*, as a function of the applied stress-intensity range, ΔK, in metallic materials, showing the regimes of primary growth-rate mechanisms and effects of several major variables on crack-growth behavior [17].

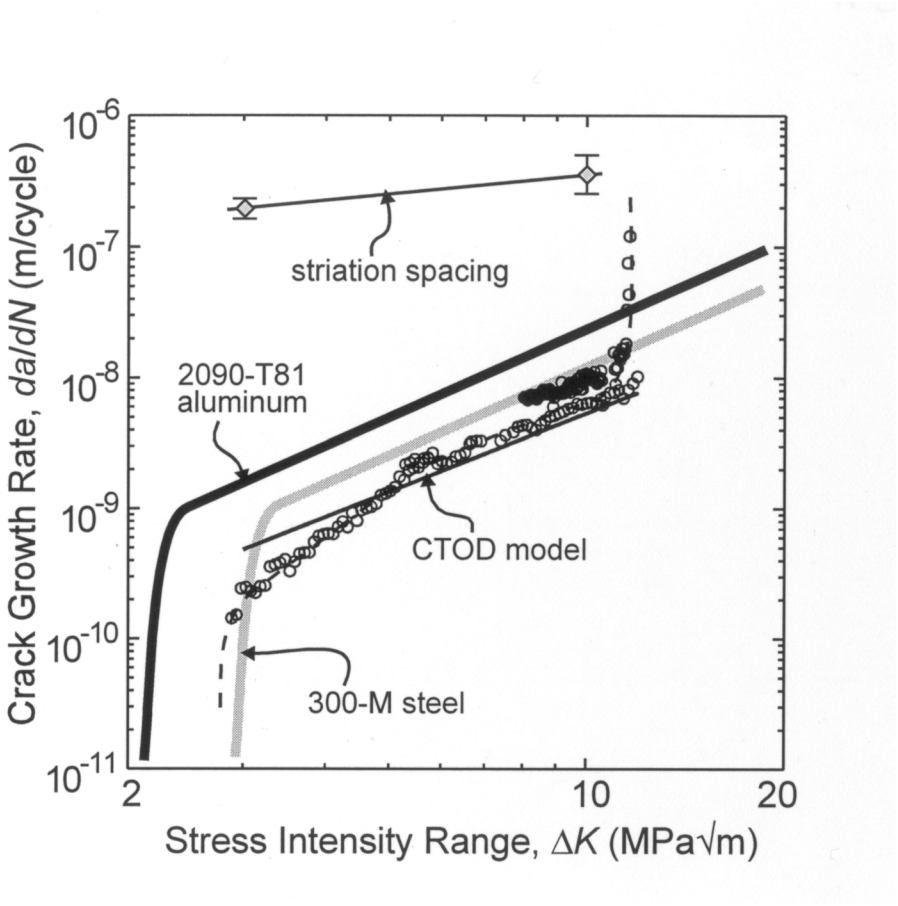

Figure 5: Fatigue-crack propagation in a bulk amorphous metal (metallic glass), $Zr_{41.2}Ti_{13.8}Cu_{12.5}Ni_{10}Be_{22.5}$, showing fatigue-crack propagation rates scaling with the ΔCTOD = 0.01 $\Delta K^2/\sigma_o E'$ (where σ_o is the flow stress and E' is the appropriate Young's modulus) and corresponding striation spacings. Also shown for comparison are growth-rate results for polycrystalline metals, namely 300-M high strength steel and 2090-T81 aluminum-lithium alloys [21].

- CRACK DEFLECTION

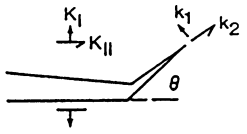

- MICROCRACK TOUGHENING:

$$\Delta(K) \sim E' f_v \varepsilon_{ii}^m \sqrt{h}$$

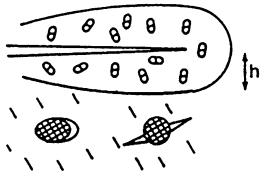

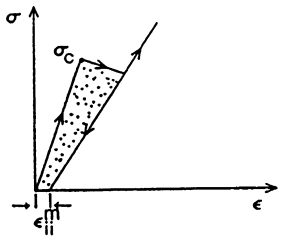

- TRANSFORMATION TOUGHENING:

$$\Delta(K) \sim E' f_v \varepsilon_{ii}^T \sqrt{h}$$

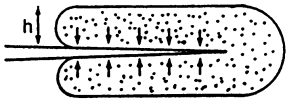

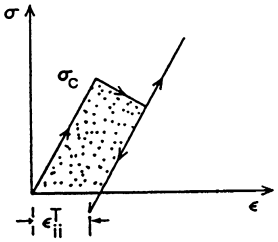

- BRITTLE FIBER/WHISKER TOUGHENING: (crack bridging)

$$\Delta(K) \sim \left(2 f_v E' \tau_i \ell^2 / \alpha\right)^{1/2}$$

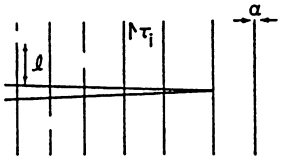

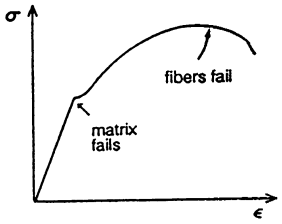

- DUCTILE PARTICLE TOUGHENING:

$$\Delta(K) \sim \left(C E' \sigma_y R f_v\right)^{1/2}$$

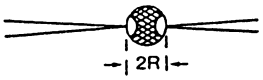

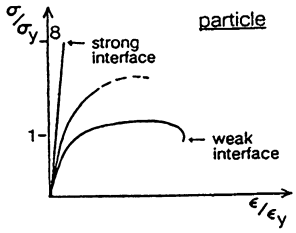

Figure 6: Schematic illustration of the primary toughening mechanisms in ceramics and ceramic-matrix composites. Note that all mechanisms are extrinsic in nature and promote inelastic deformation which results in a nonlinear stress/strain relationship.

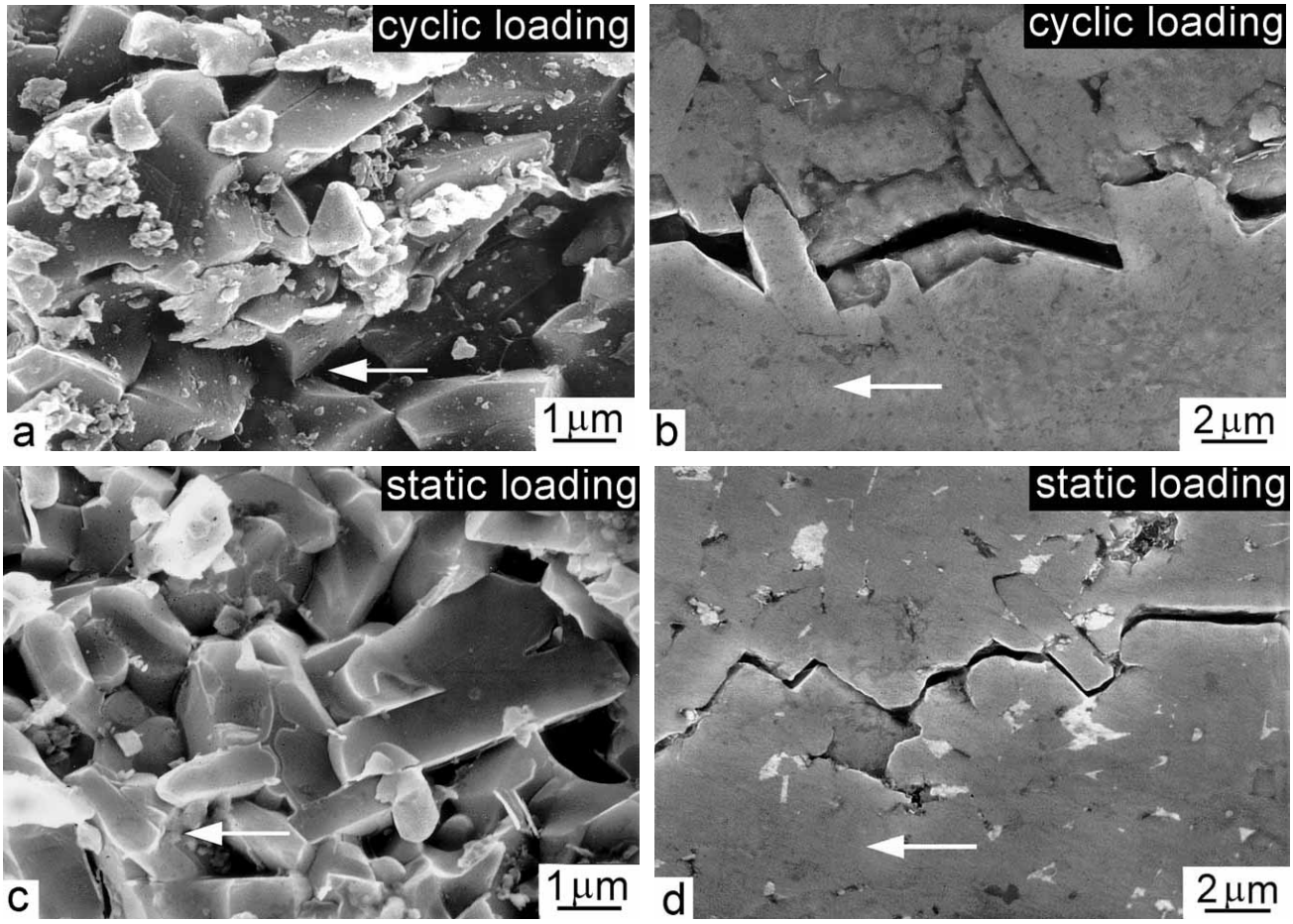

Fig. 7: Fractography of ceramic fatigue in an *in situ* toughened silicon carbide (ABC-SiC) at ambient temperatures showing the fractography and crack trajectories under (a,b) cyclic and (c,d) static loading. Note the nominally identical intergranular fracture surfaces in (a) fatigue and c) on the R-curve, and associated crack-tip shielding by grain bridging (b,d) in the crack wake. Due to repetitive opening and closing of the crack, such bridging leads to the creation of more debris and surface damage on the fatigue surfaces in fatigue [30]. Horizontal arrow represents direction of crack growth.

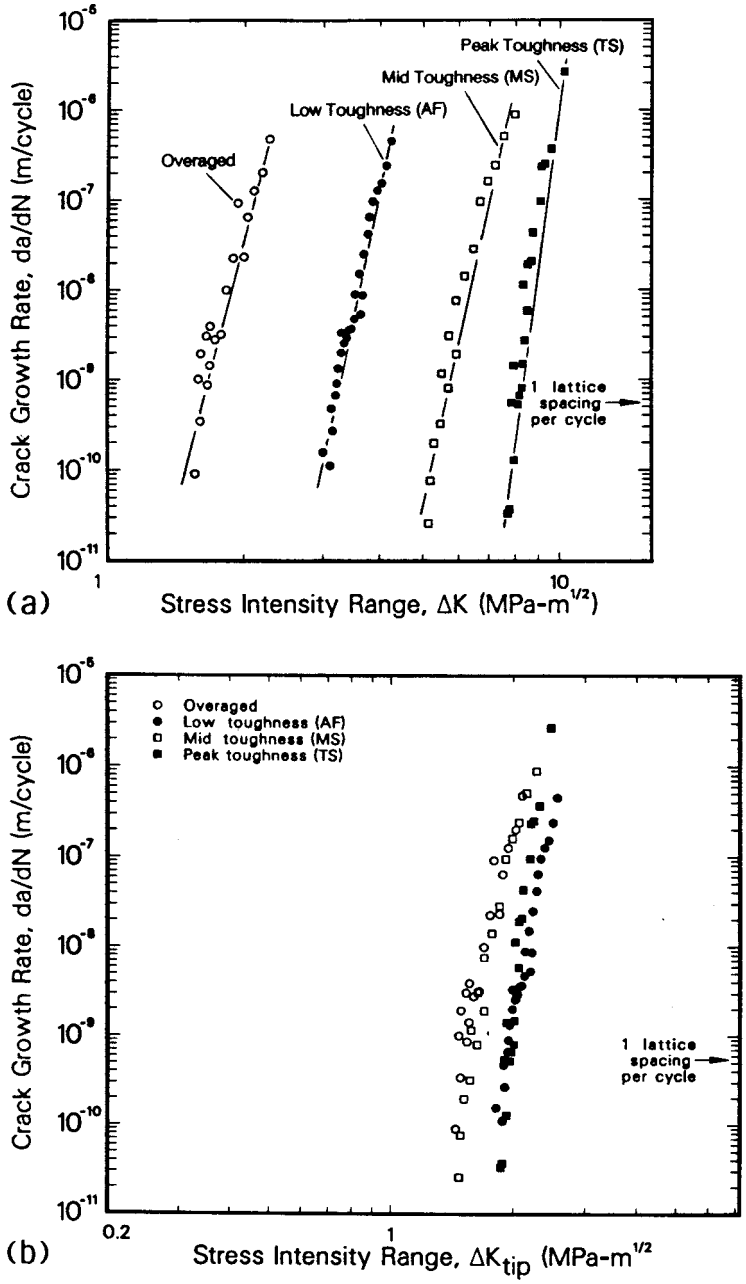

Figure 8: Fatigue-crack growth rates, *da*/*dN*, for a range of transformation-toughened partially-stabilized zirconias (Mg-PSZ), as a function of (a) the applied stress-intensity range, ΔK, and (b) the effective, near-tip stress intensity, ΔK_{tip}, which is equivalent to the maximum stress intensity normalized by the fracture toughness, K_{max}/K_c [7].

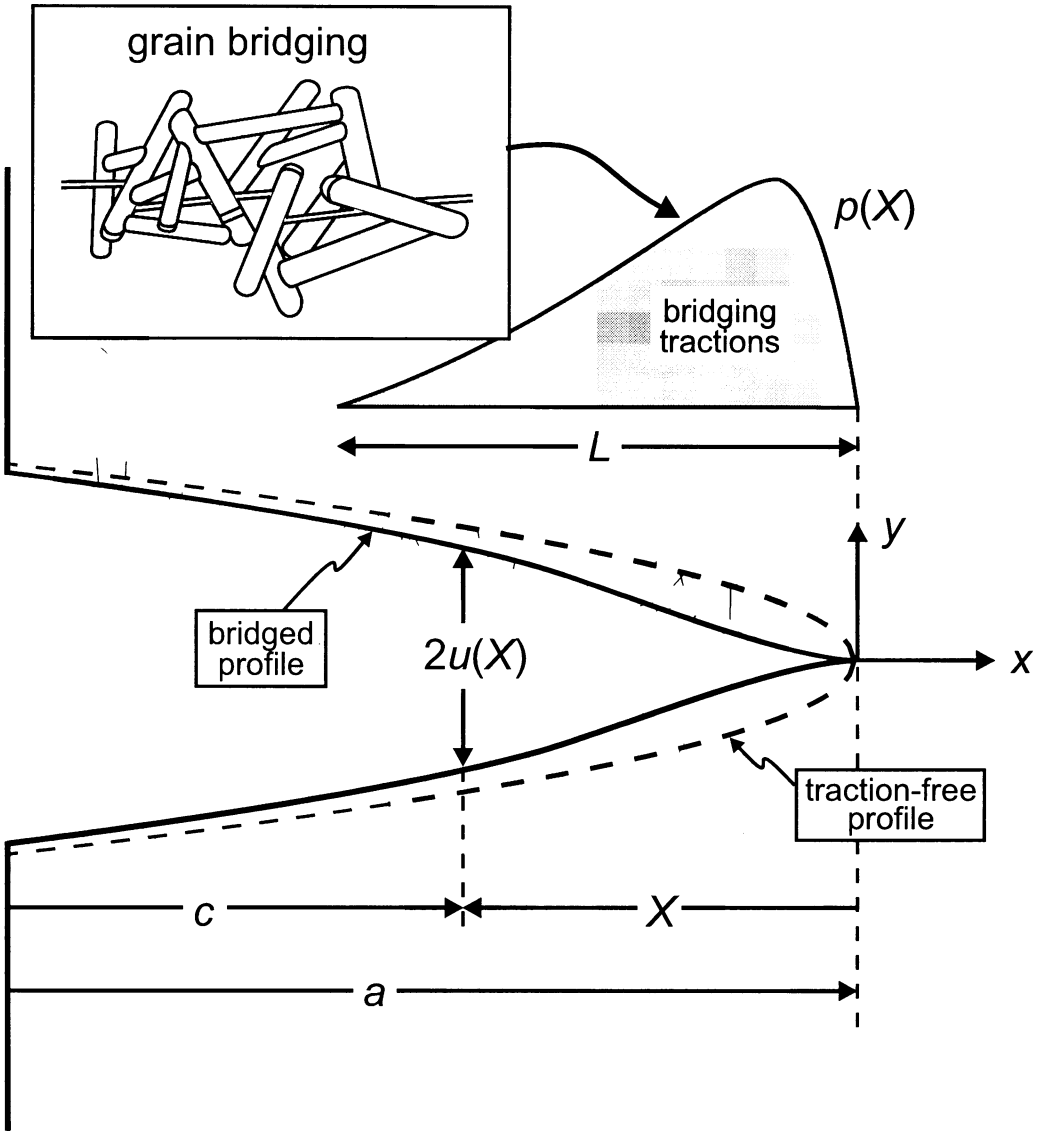

Fig. 9: Crack-tip shielding from bridging by interlocking grains (inset) showing (b) the variation in bridging tractions $p(X)$ due to debonding and frictional pullout, and the corresponding crack-opening profile, as a function of the crack opening displacement ($2u$) [42]. Under cyclic loading, the bridging is observed to decay, i.e., *p(u)* is progressively decreased.

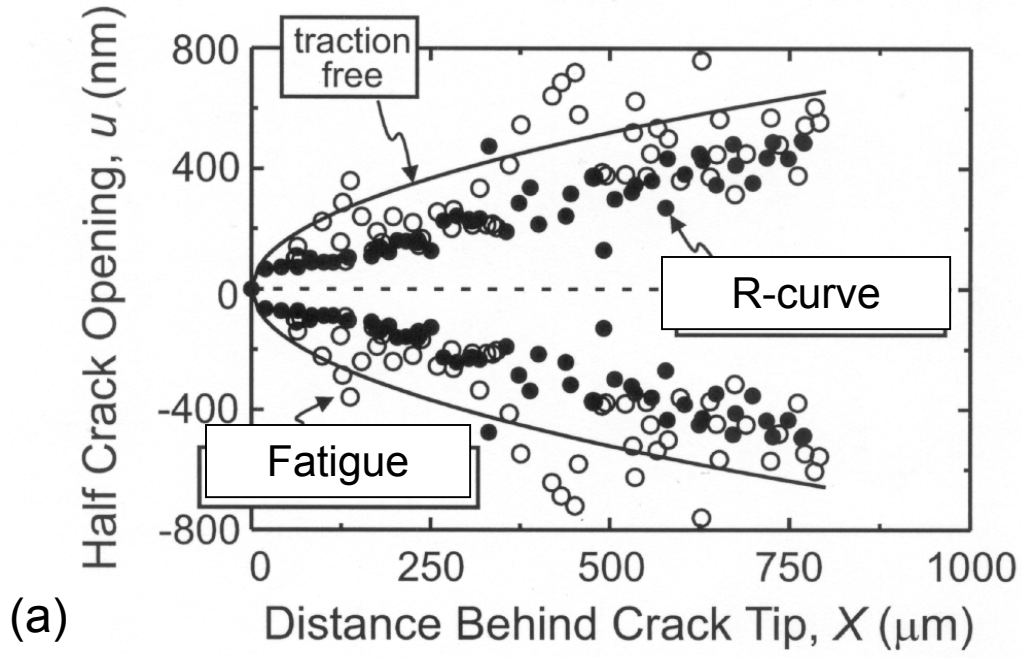

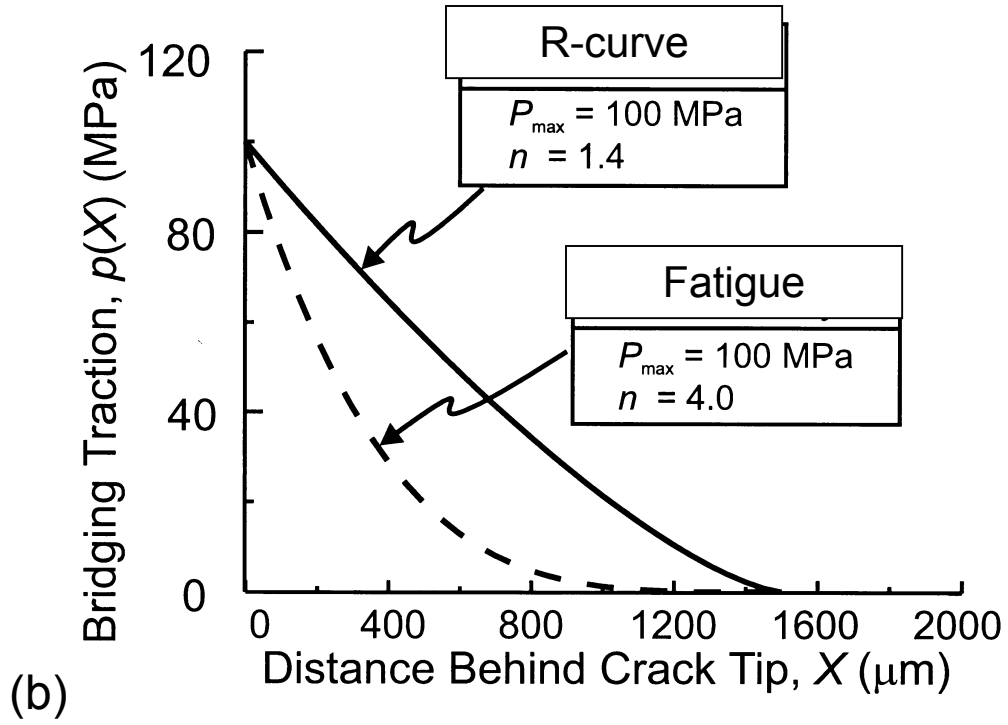

Fig. 10: Measured crack-opening profiles in an ABC-SiC ceramic for (a) where the crack was grown near instability (on the R-curve), and where the crack was grown in fatigue near threshold (at ~1 x 10^{-10} m/cycle at ~75% K_c). In (b), the best-fit bridging traction distributions are plotted for each case [41].

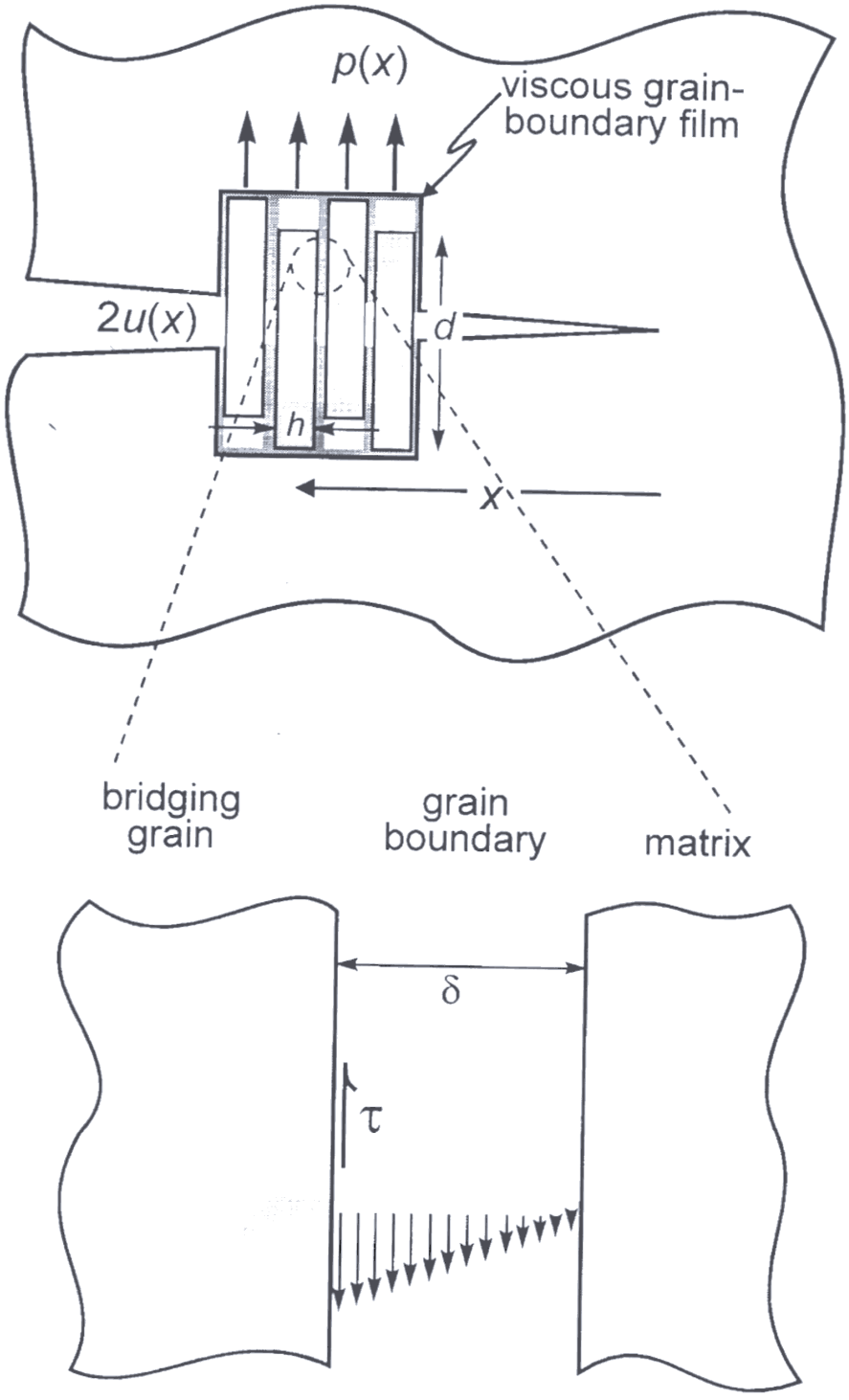

Figure 11: Model for crack-tip shielding at higher temperatures from viscous grain-boundary film bridging, showing the development of the viscous force resulting from the velocity gradient in the film [61].

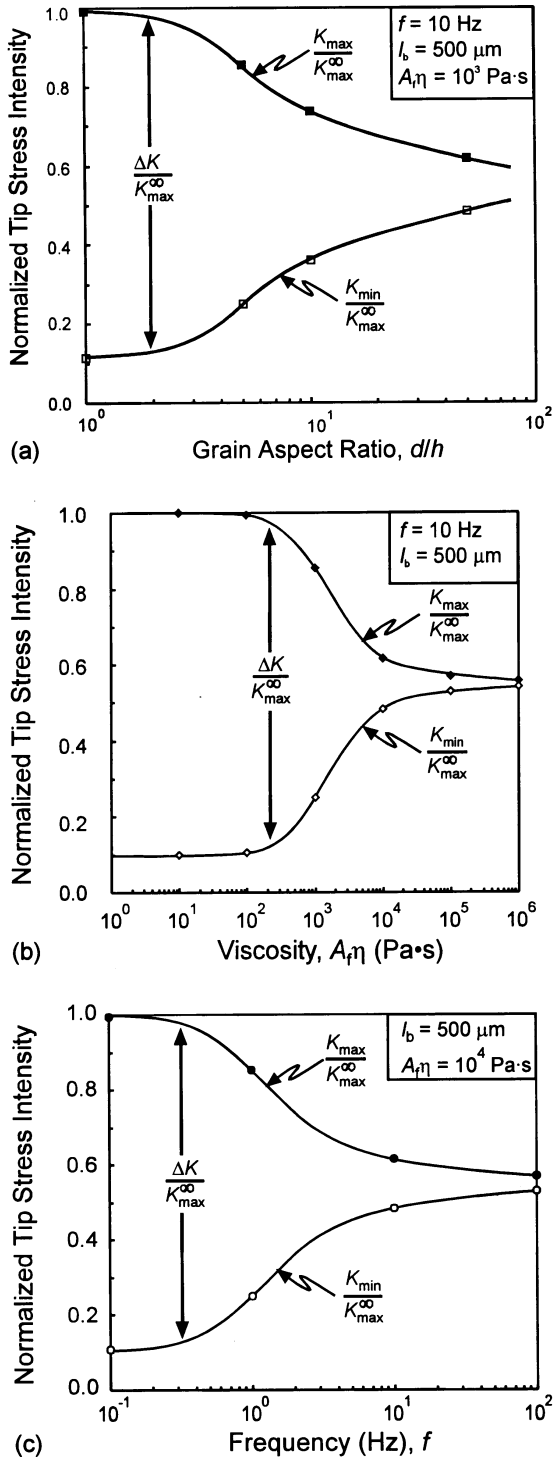

Figure 12: Self-consistent solution results showing predicted variations in the maximum, K_{max}, and minimum, K_{min}, crack-tip stress intensity, normalized to the maximum applied stress intensity, K^{∞}_{max}, versus changes in the model parameters, namely (a) grain aspect ratio, d/h, (b) viscosity, η, and (c) frequency, f. The normalized crack-tip stress intensity range, $\Delta K / K^{\infty}_{max}$, is shown as the difference between the two curves [61].

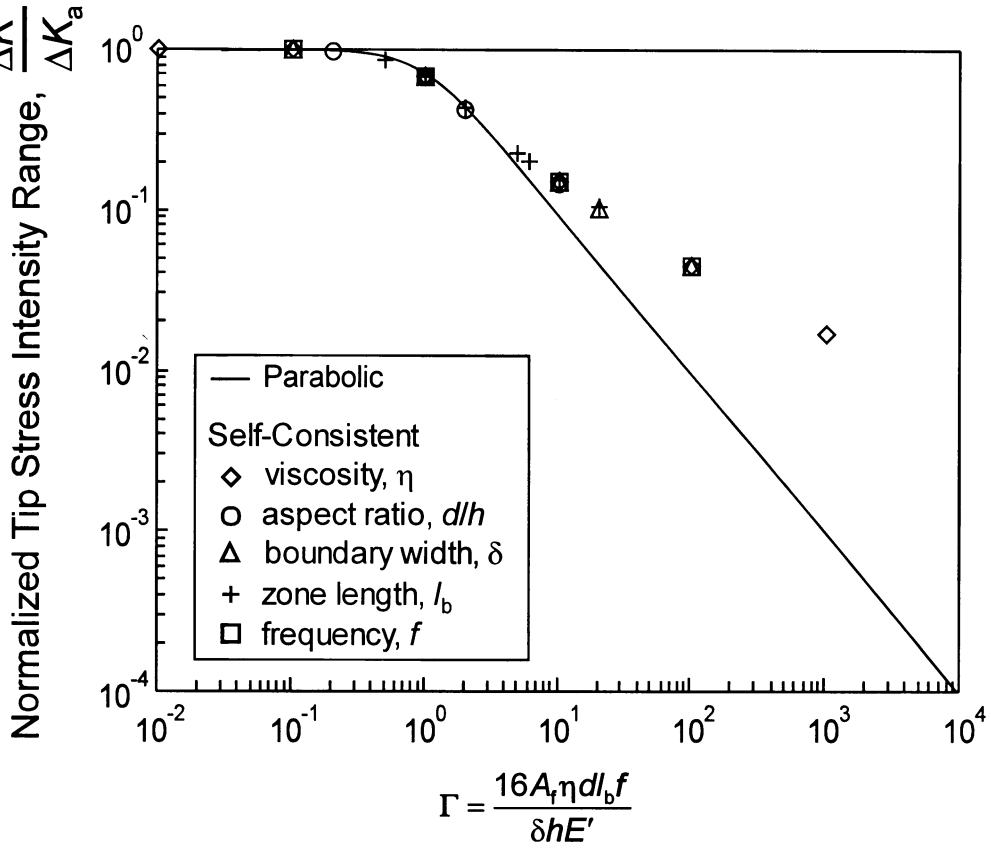

Figure 13: Self-consistent solution results showing variations the crack-tip stress-intensity range, ΔK, normalized by the applied stress-intensity range, ΔK_a, versus the non-dimensional parameter Γ. Changes in the individual parameters of the model are shown by symbols while the parabolic solution is denoted by the solid line. Note that the self-consistent solution, which diverges from the parabolic at high Γ, is well-represented over the entire range by Γ [61].

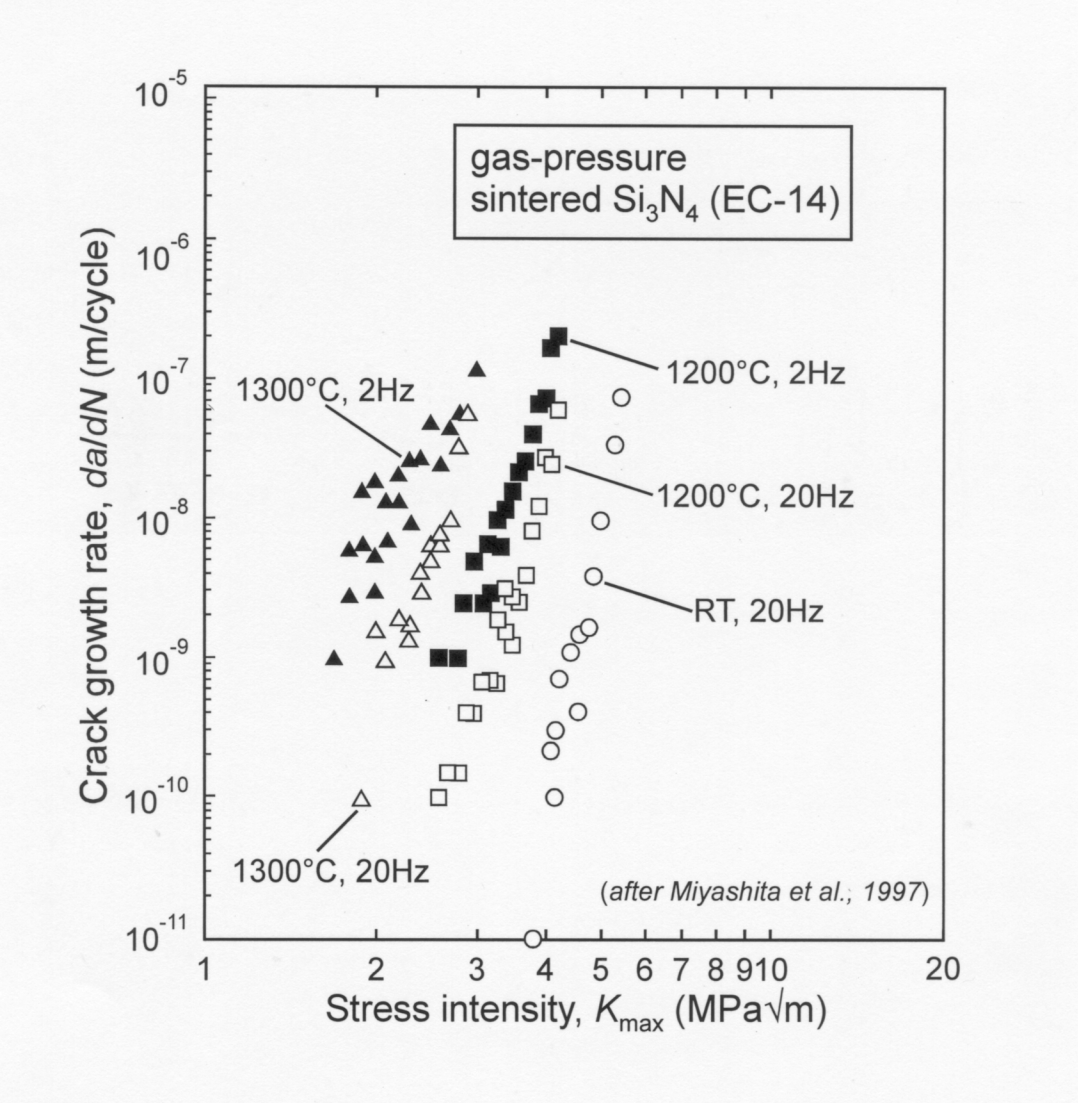

Figure 14:Effect of cyclic frequency (2-20 Hz) on cyclic fatigue-crack growth rates, as a function of K_{max}, in gas-pressure sintered silicon nitride (EC-14) at 1200° and 1300°C, as compared to 20 Hz data at room temperature [62].

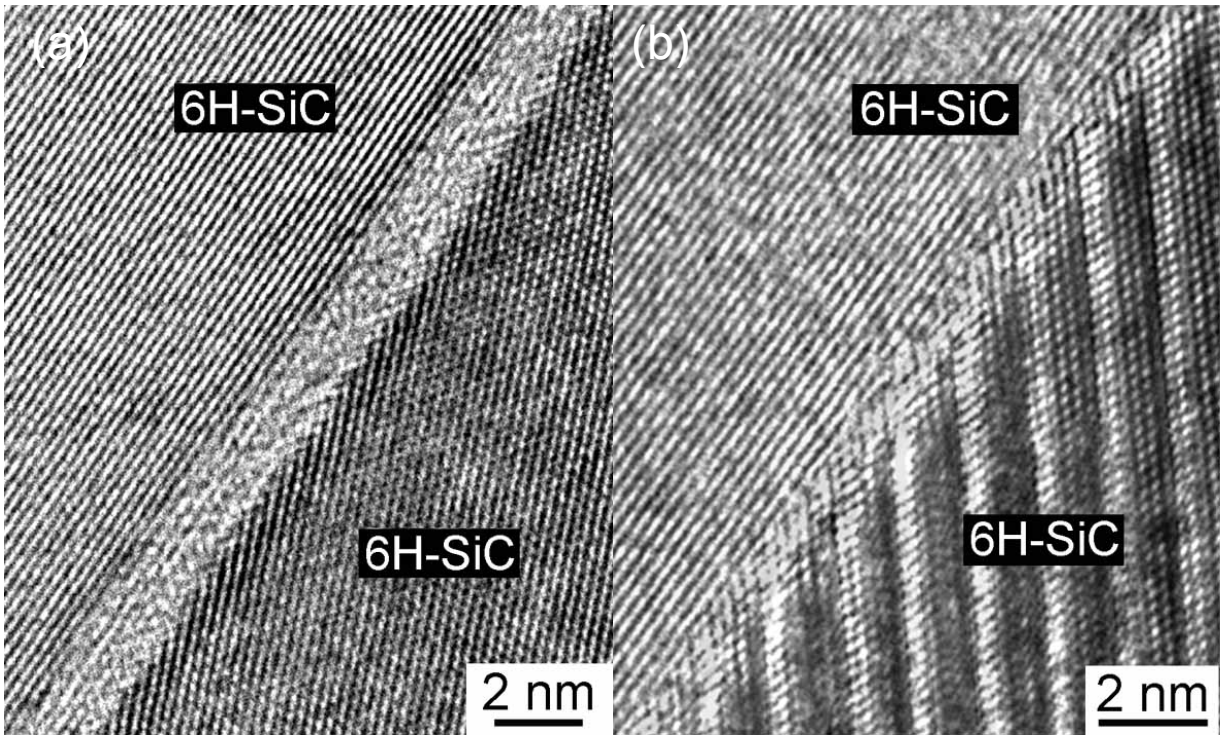

Figure 15. High-resolution transmission electron micrographs of the grain boundaries in ABC-SiC in the (a) as-processed, and (b) thermally exposed (1300°C for ~ 72 hr) conditions. Note the complete crystallization of the amorphous phase after exposure compared to the glass film of ~ 1 nm under as-processed condition [30].

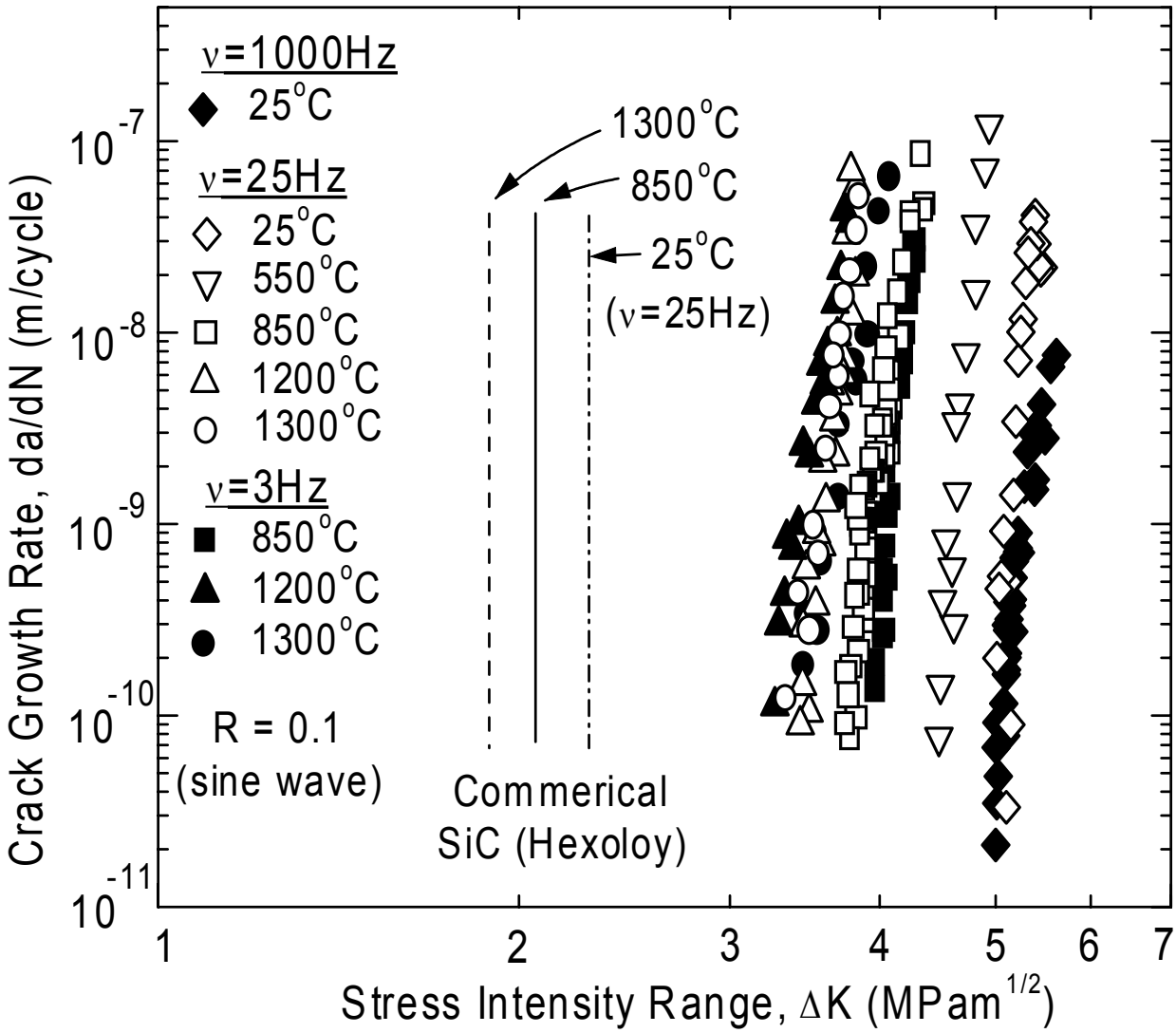

Figure 16. Cyclic fatigue-crack growth rates, d*a*/d*N*, in ABC-SiC as a function of the applied stress-intensity range Δ*K* for the tests conducted at temperatures between 25° and 1300°C, load ratio *R* = 0.1, and frequencies between 3 and 1000 Hz. For comparison, the crack growth behavior of commercial SiC (Hexoloy) is also illustrated [30,63].

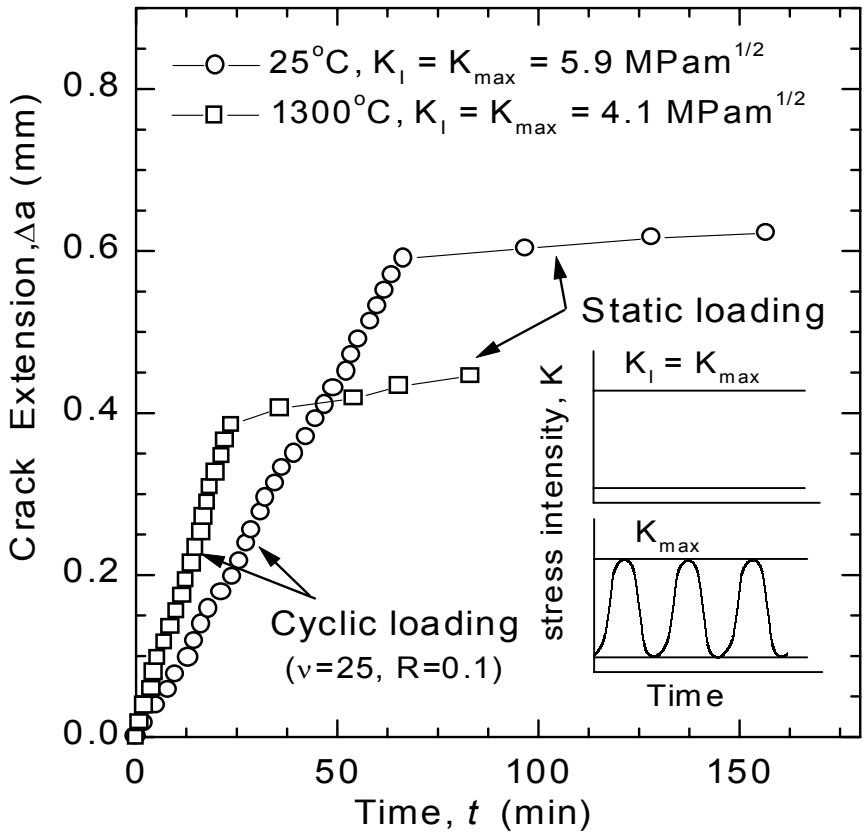

Figure 17. Crack extension, Δa, plotted as function of time, t, in ABC-SiC demonstrating the effect of sustained loading vs. cyclic loading conditions, at a fixed maximum stress intensity ($K_I = K_{max}$). Plotted is behavior at 25°C, where $K_I = K_{max} = 5.9$ MPa√m, and at 1300°C, where $K_I = K_{max} = 4.1$ MPa√m [30,63].

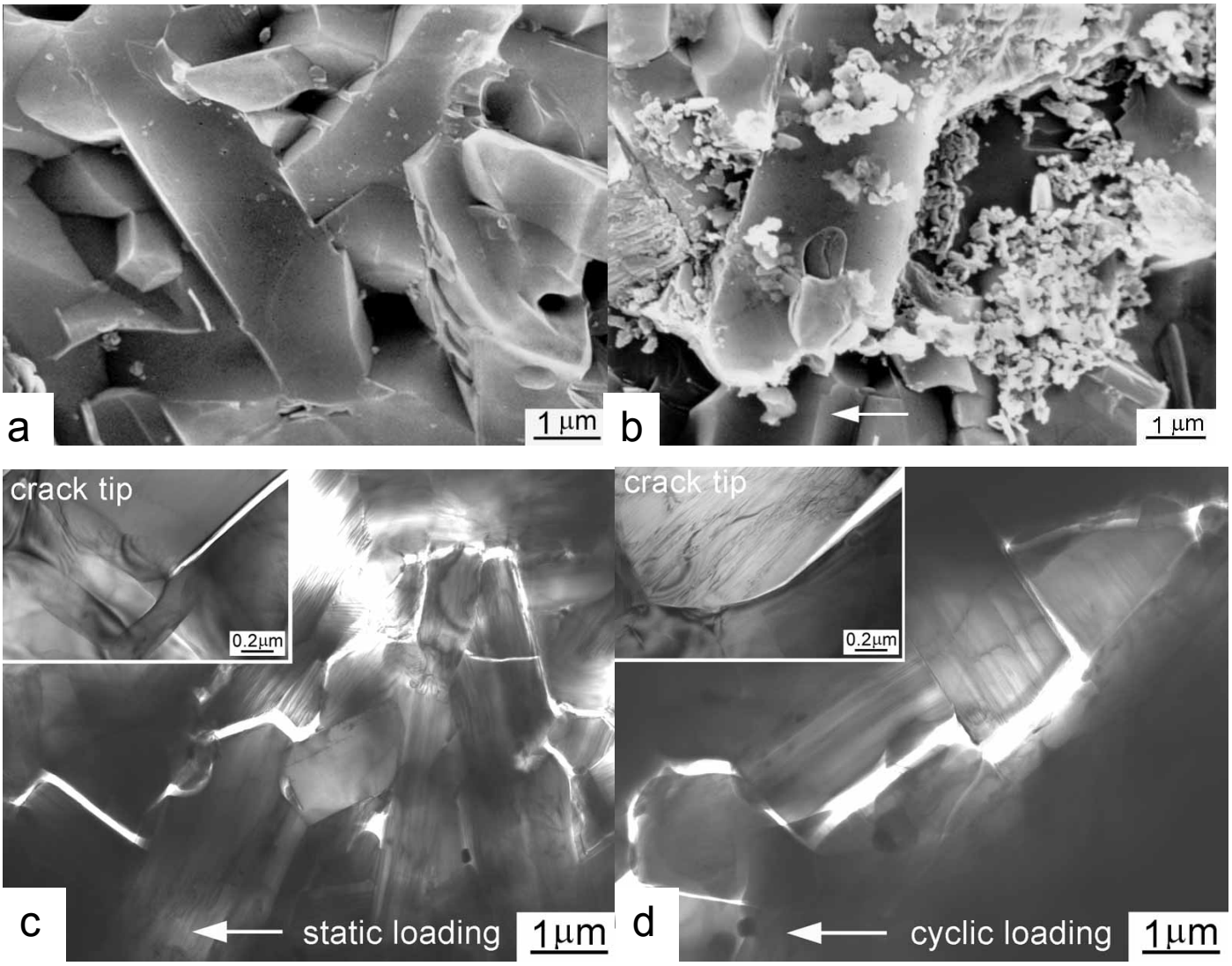

Figure 18. Comparison of crack growth under sustained (static) and cyclic fatigue loading ABC-SiC at elevated temperatures (1300°C), showing scanning electron micrographs of the fracture surfaces under (a) sustained and (b) cyclic loads, and transmission electron micrographs of the crack profiles at the crack-tip region in under (c) sustained loading (K_I = 4.1 MPa√m) and (d) cyclic fatigue loading (R = 0.1, ν = 25 Hz, K_{max} = 4.1 MPa√m). Arrows indicate the general direction of crack propagation [30].

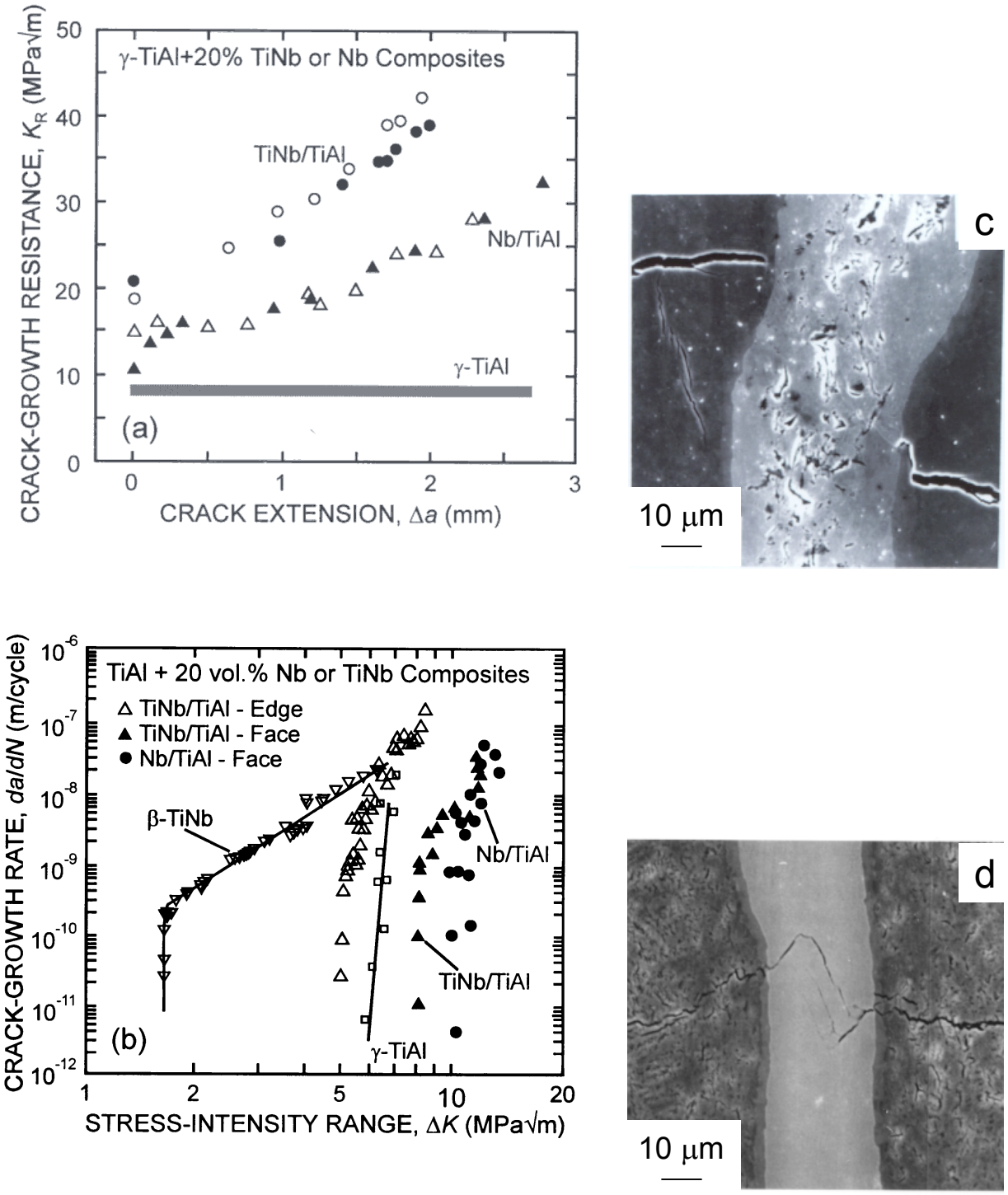

Figure 19.(a) Fracture toughness and (b) fatigue-crack growth behavior in a 20 vol.% TiNb-reinforced γ-TiAl intermetallic composite at 25°C at R = 0.1 in the edge (C-R) and face (C-L) orientations, where the results are compared to data for pure γ-TiAl, β-TiNb and a Nb-particulate reinforced γ-TiAl composite. (c) Extensive crack bridging by the uncracked ductile phase under monotonic loading is severely degraded under cyclic loading due to (d) premature fatigue failure of the ductile ligaments [34,35].

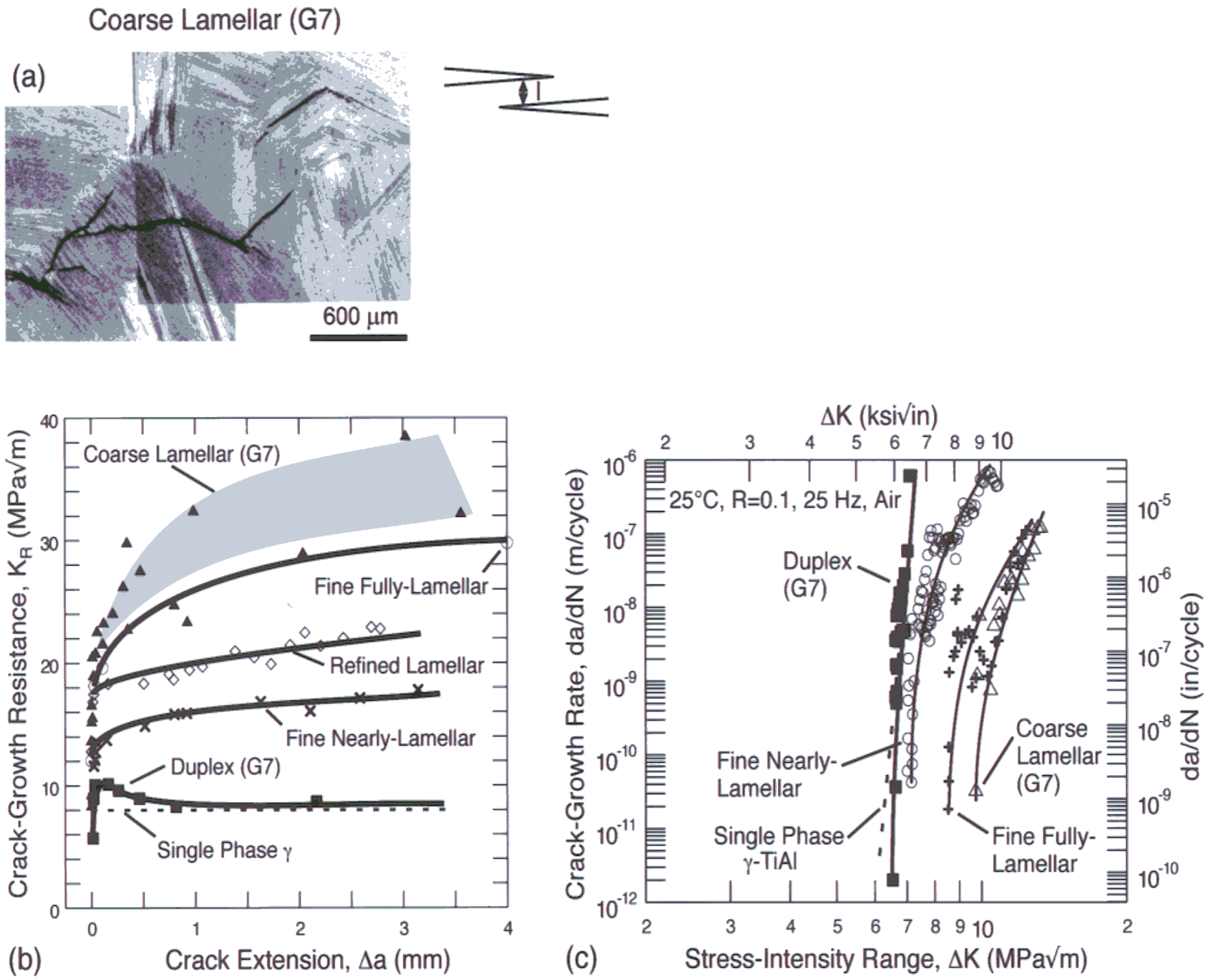

Figure 20.(a) Crack-tip shielding by uncracked (shear) ligament bridging in ($\gamma+\alpha_2$) titanium aluminide (e.g., Ti-47wt.%Al) alloys promotes excellent (b) R-curve toughening and (c) fatigue-crack growth resistance (compared to single-phase γ), particularly in the coarser lamellar microstructures. Such bridging does degrade under cyclic loading; however, the uncracked ligaments do not necessarily fail preferentially (as in ductile-phase bridging) as they are the same material as the matrix [82].

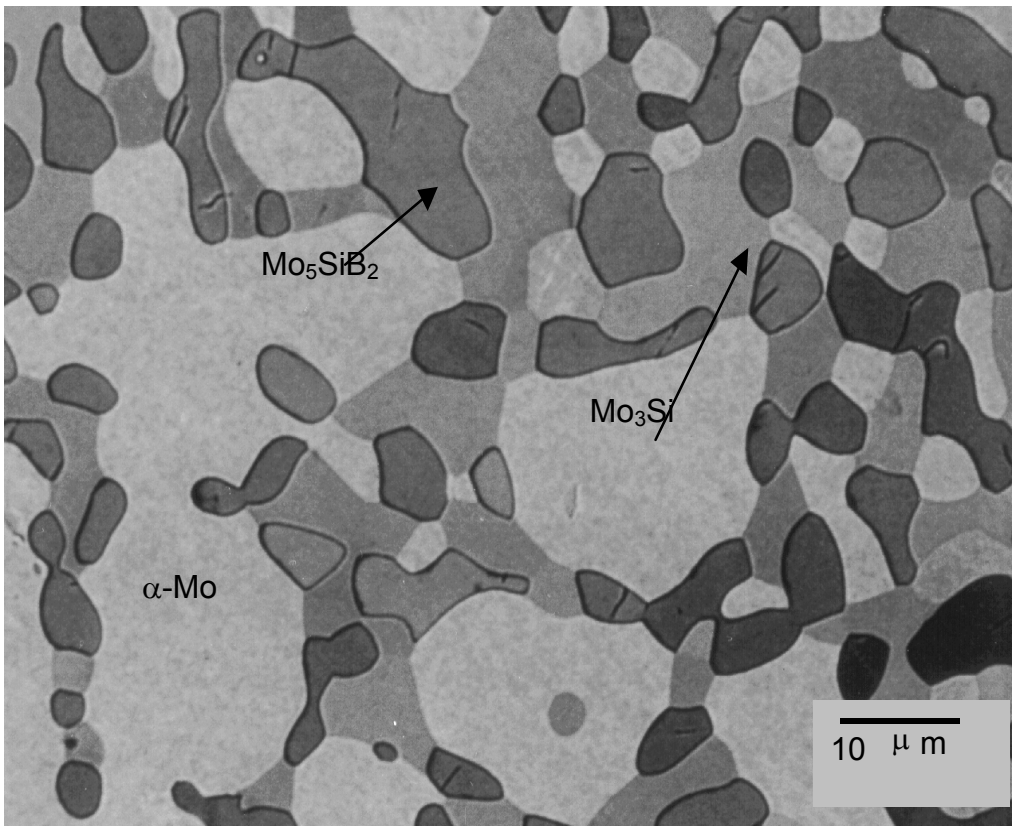

Figure 21. Scanning electron micrograph of the microstructure in the I/M Mo-12Si-8.5B (at.%) refractory silicide alloy, showing coarse α-Mo particles in an intermetallic matrix of Mo_3Si and Mo_5SiB_2 (T2) phases. (Etchant: Murakami's reagent) [84].

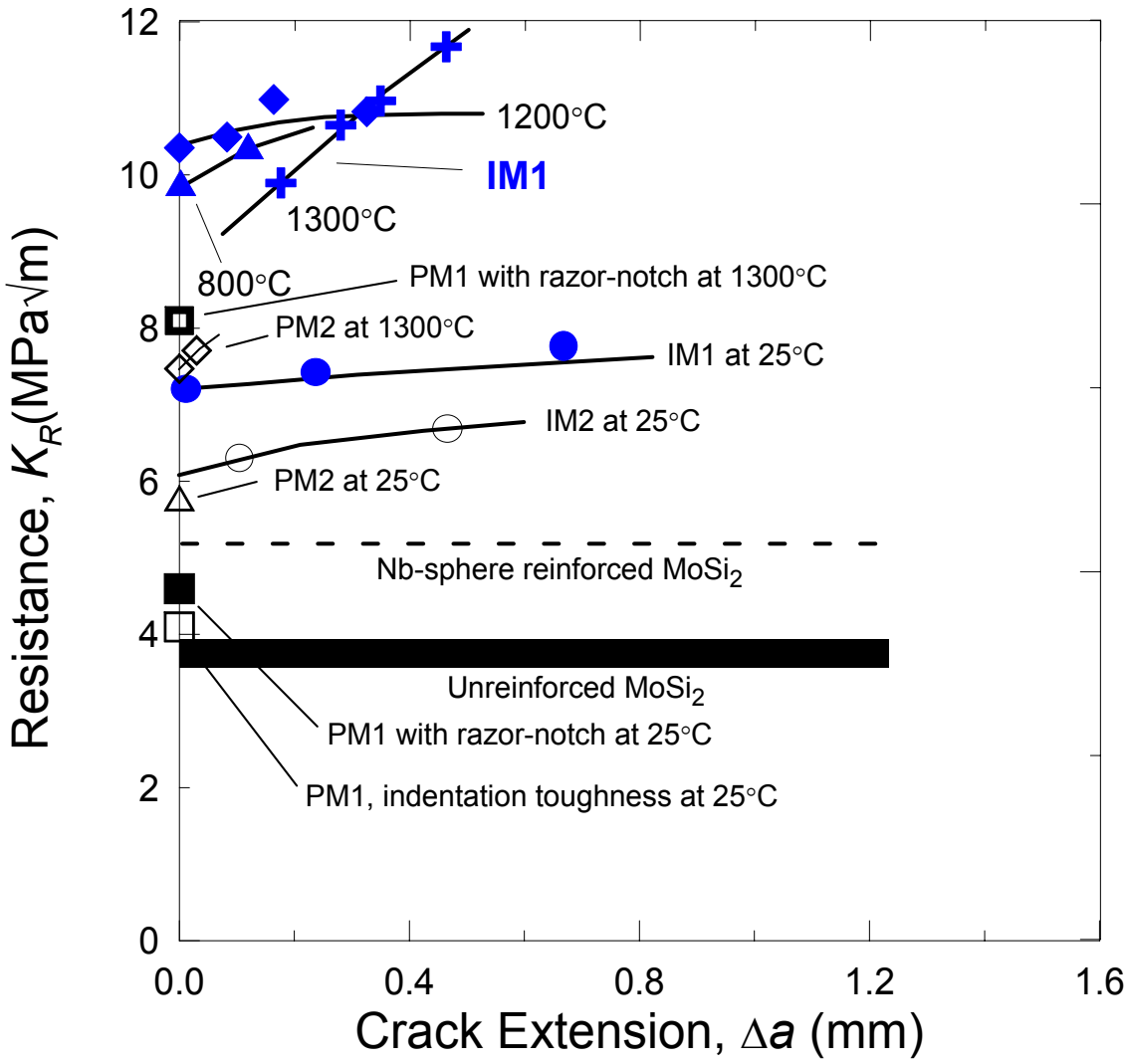

Figure 22. Fracture toughness in the form of R-curve behavior for a series of I/M and P/M Mo-Si-B alloys, showing crack-growth resistance, K_R, plotted as a function of crack extension, Δa, for the I/M and P/M alloys between 25° and 1300°C. IM1 and IM2 are I/M alloys with composition (at.%) Mo-12Si-8.5B and Mo-12Si-10Nb-8.5B, respectively; PM1 and PM2 are P/M alloys both with composition (at.%) Mo-16.8Si-8.4B. Results for the boron-modified molybdenum silicides are compared with previous data [74] on monolithic and Nb-particulate reinforced $MoSi_2$ [84,85].

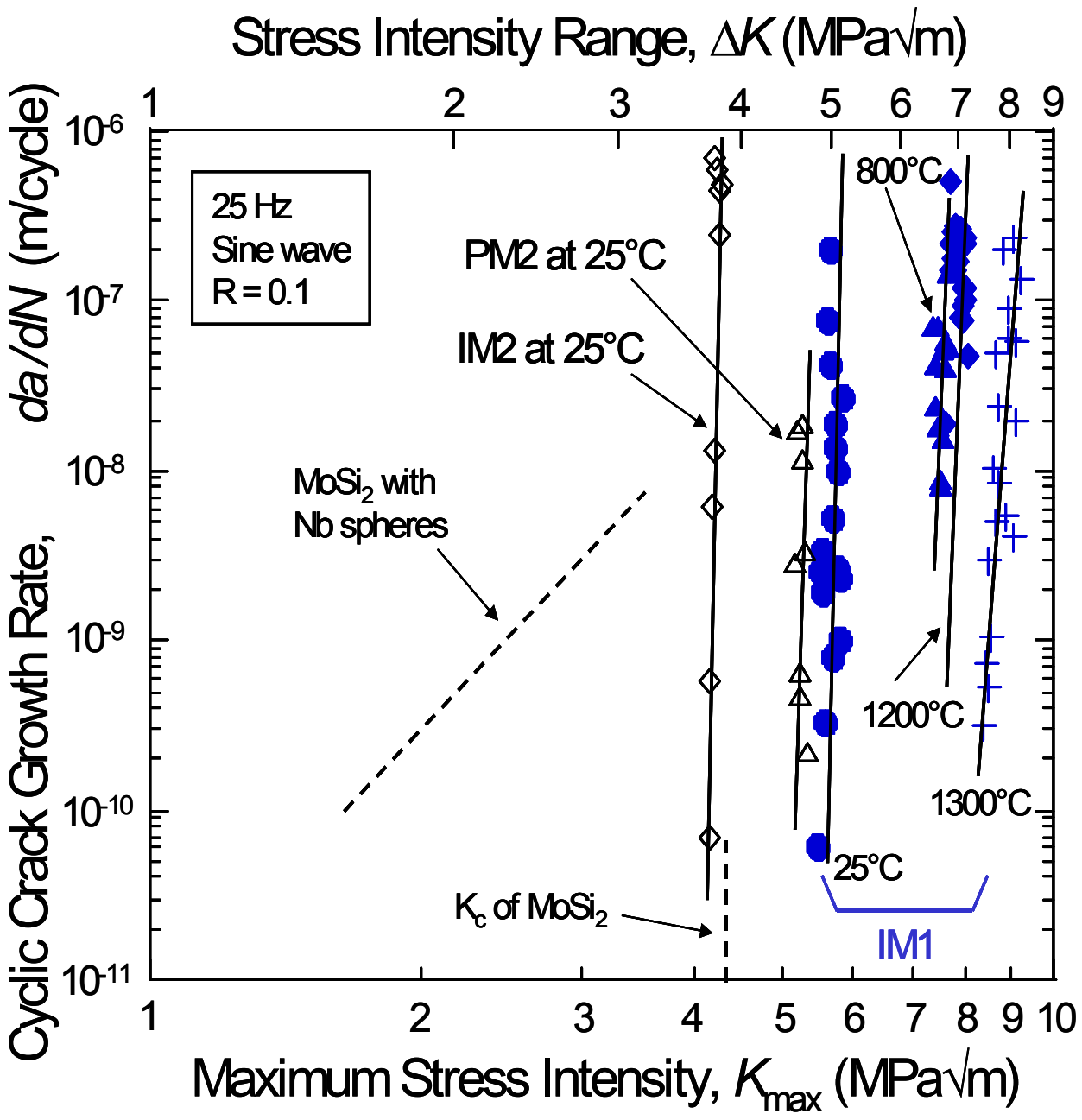

Figure 23. Variation in cyclic fatigue-crack propagation rates, d*a*/d*N*, as a function of the applied maximum, K_{max}, and alternating, ΔK, stress intensities, in the same series of boron-modified molybdenum silicide alloys shown in Figure 22, at a load ratio *R* of 0.1 between 25° and 1300°C [84,85]. Shown for comparison are previous results [74] for Nb-particulate reinforced $MoSi_2$.

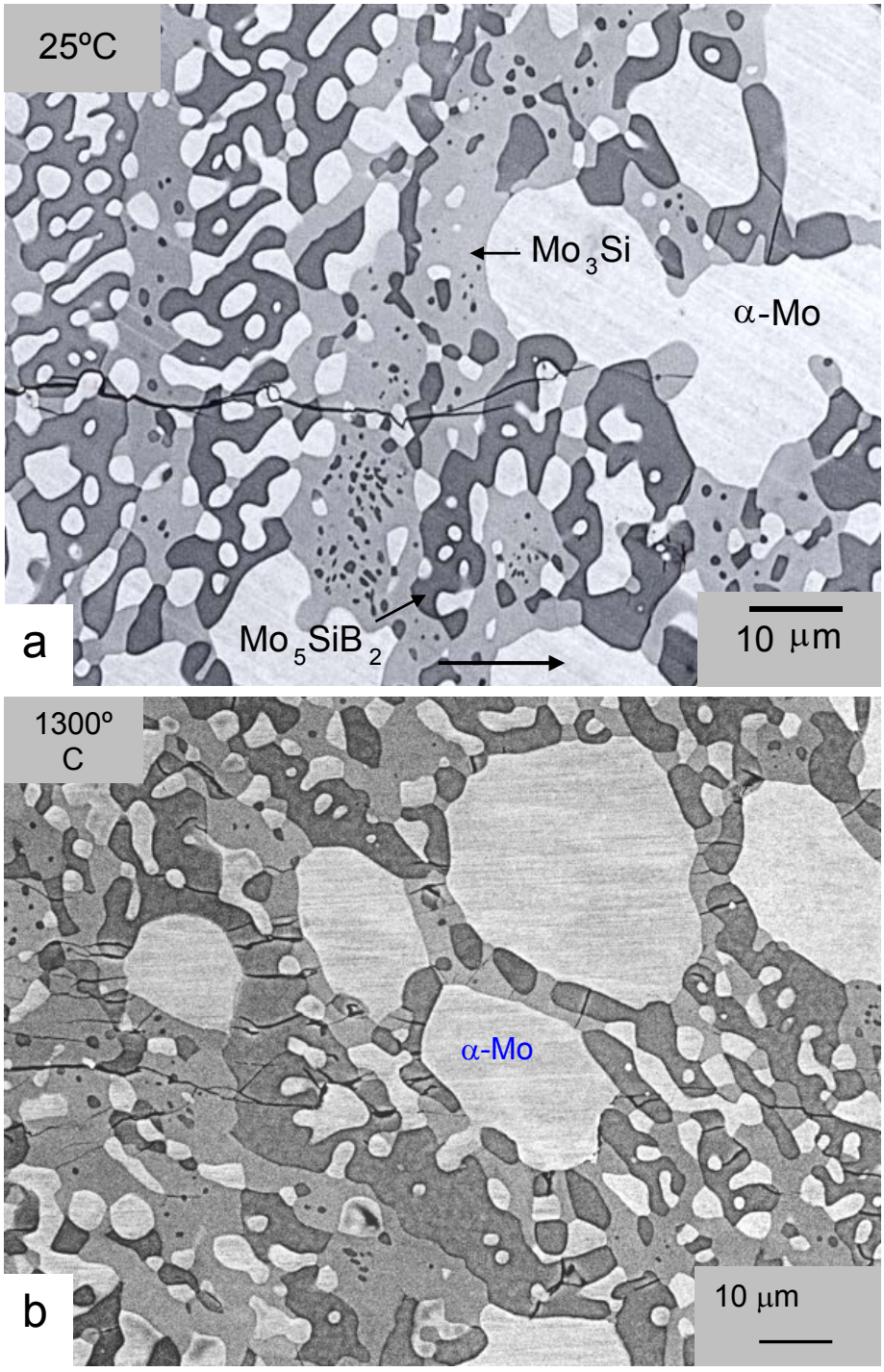

Figure 24. The interaction of crack path with the microstructure in an I/M Mo-12Si-8.5B alloy (IM1). In (a), crack arrest occurs at a large (~ 30 μm) α-Mo particle at 25°C; whereas the main crack readily propagates through, or around, the smaller Mo particles, the larger particles act as significant crack traps. In (b), extensive microcracking, primarily in the Mo_5SiB_2 phase, is seen parallel to the main crack at 1300°C. Horizontal arrow represents direction of crack growth [84,85].

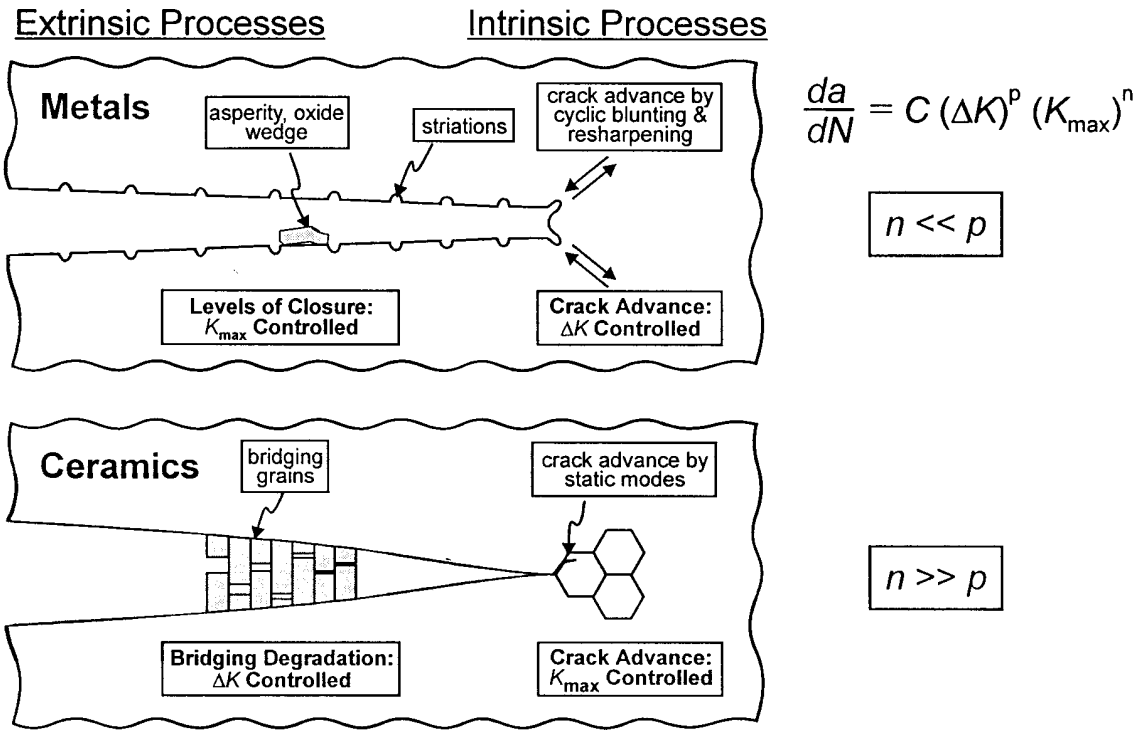

Figure 25. Schematic illustrations of the intrinsic and extrinsic mechanisms involved in cyclic fatigue-crack growth in (a) metals and (b) ceramics, showing the relative dependencies of growth rates, da/dN, on the alternating, ΔK, and maximum K_{max}, stress intensities [9].